

JGR Planets

REVIEW ARTICLE

10.1029/2025JE009139

Key Points:

- Overview of the structure and composition of planetary crusts
- Discussion on how gravity and topography data can be used to constrain crustal thickness
- Suggestion of improvements to crustal thickness modeling, including the consideration of the gravity field resolution and data filtering

Supporting Information:

Supporting Information may be found in the online version of this article.

Correspondence to:

A. Broquet, adrien.broquet@dlr.de

Citation:

Broquet, A., Maia, J., & Wieczorek, M. A. (2025). On the crustal architecture of the terrestrial planets. *Journal of Geophysical Research: Planets*, *130*, e2025JE009139. https://doi.org/10.1029/2025JE009139

Received 15 APR 2025 Accepted 21 AUG 2025 Corrected 11 SEP 2025

This article was corrected on 11 SEP 2025. See the end of the full text for details.

Author Contributions:

Conceptualization: A. Broquet
Data curation: A. Broquet
Formal analysis: A. Broquet
Investigation: A. Broquet
Methodology: A. Broquet
Resources: A. Broquet
Software: A. Broquet
Validation: A. Broquet
Visualization: A. Broquet
Writing – original draft: A. Broquet
Writing – review & editing: A. Broquet,
J. Maia, M. A. Wieczorek

© 2025. The Author(s). This is an open access article under the terms of the Creative Commons Attribution License, which permits use, distribution and reproduction in any medium, provided the original work is properly cited.

On the Crustal Architecture of the Terrestrial Planets

A. Broquet¹, J. Maia¹, and M. A. Wieczorek²



Abstract Understanding the structure and composition of planetary crusts is fundamental for unraveling the diverse geologic pathways of rocky bodies in the solar system. In recent years, geophysical missions have shed light on the crustal architecture of the Moon and Mars. New missions are currently en route to Mercury and in preparation for Venus. Here, we provide an overview of our current knowledge of the crustal structure of the Moon, Mars, Mercury and Venus, and present nominal models for these planets. Planetary crusts are thought to have average thicknesses of ~20 km (Venus), ~30 km (Mercury, Moon) and higher (30–70 km, Mars), and generally represent a few percent of the silicate mass fraction of their planet. In comparison, crustal thickness on Earth is bimodal, with values of 40 and 7 km for the continental and oceanic crusts, respectively, for a global average of ~19 km. We highlight that gravity inversions must account for the often-uneven resolution of gravity fields and show that the classical Bouguer anomaly filtering step can be avoided by simultaneously inverting for crustal density and thickness. Rather than discarding data, this method ascribes short-wavelength gravity anomalies to crustal density variations. For Mercury, Venus, and the Moon, we discuss the effect of having a laterally variable mantle density on crustal thickness inversions, and for Mars, we present an approach to consider a high-density basaltic crust. While crustal thickness inversions remain non-unique, we discuss that the distribution of tectonic and volcanic landforms can help constrain the range of plausible models.

Plain Language Summary The crust is the outermost tens of kilometer-thick solid layer of a rocky planet. The crust represents a physical boundary that dictates the rate at which the interior cools in time as well as how volcanic, tectonic, or impact cratering processes are expressed at the surface. Thus, the shape and composition of the crust hold fundamental information on the geologic history of a planet. The structure of planetary crusts is typically inverted using observed gravity and topography data, and, when available, seismic data. In recent years, geophysical missions have shed considerable light on the interior structure of the Moon and Mars. New space missions are currently en route to Mercury and in preparation for Venus. Here, we provide an overview of our current knowledge of the crustal structure of the Moon, Mars, Mercury, and Venus. We summarize the different geophysical approaches to estimate crustal thickness and present nominal models for the terrestrial planets. Crusts are thought to have average thicknesses of ~20 km (Venus), ~30 km (Mercury, Moon), and higher (30–70 km, Mars). While crustal thickness inversions remain non-unique, we argue that geologic data, including the distribution of tectonic and volcanic landforms, can help constrain the range of plausible models.

1. Introduction

The crust is the outermost solid layer of a rocky body that sets the stage for the planet's geologic evolution. The crust acts as a physical boundary that thermally insulates the interior, thereby determining the rate at which a planet cools in time (Plesa et al., 2022). The thickness and rigidity of the crust further control how volcanic (e.g., Broquet & Wieczorek, 2019), tectonic (e.g., Watters et al., 2021), or impact cratering processes (e.g., Miljković et al., 2013) are expressed at the surface. The crust preserves a record of planetary history, from dynamos (e.g., Langlais et al., 2010), tectonic contraction (e.g., Andrews-Hanna & Broquet, 2023), giant impacts (e.g., Melosh et al., 2013) and erosion (e.g., Hynek et al., 2010) to geologically recent volcanic eruption (e.g., Carr & Head, 2010). Being compositionally distinct from the mantle and core, the thickness of the crust is also critical for understanding the bulk composition of the body (e.g., Taylor & McLennan, 2009; Taylor & Wieczorek, 2014). Thus, understanding the structure and composition of the crust is fundamental for uncovering the diverse geologic pathways of rocky bodies in the solar system. In this work, when discussing common geologic processes that operate on planetary bodies, we will refer to Earth's Moon as a planet (Metzger et al., 2022).

BROQUET ET AL. 1 of 28

Planetary crusts vary widely in shape and thickness as a result of different formation mechanisms and evolutionary histories. On Earth, the contrast between the older, thicker, and lower-density continental crust compared to the oceanic crust reflects the complex interplay of large-scale interior dynamics and plate tectonics with local alteration and magmatic processes (e.g., Spencer et al., 2017). Decades of space research demonstrated, however, that having a mobile and fragmented crust as on Earth is the exception rather than the norm. Mercury, the Moon and Mars are currently in a stagnant lid regime, where the crust is unlikely to have been reincorporated into the mantle in any substantial amount (though see Michalski et al., 2024 discussing crustal recycling on early Mars). Giant basins engraved in the crusts of stagnant lid bodies bear witness to the early orbital chaos in the Solar System (e.g., Fassett & Minton, 2013), while extensive flood volcanism marks the remnants of geodynamically active planetary interiors at the dawn of their histories (e.g., Byrne, 2020). While Venus does not have plate tectonics at present-day, the planet's lithosphere, encompassing the crust and potentially part of the upper mantle, might have been recycled at regional scale (e.g., Lourenço et al., 2020) or was subject to global recycling events in the past (e.g., Armann & Tackley, 2012). Venus's mobile- or squishy lid regime allows for enhanced surface mobility in comparison to the stagnant lid planets.

In the last few years, important progress has been made in our understanding of planetary crusts, with the Gravity Recovery And Interior Laboratory (GRAIL) sounding the lunar interior (e.g., Wieczorek et al., 2013; Zuber et al., 2013) and InSight characterizing the internal structure of Mars (e.g., Banerdt et al., 2020; Knapmeyer-Endrun et al., 2021). Major advances are also on the horizon, with the EnVision and the Venus Emissivity, Radio Science, InSAR, Topography, and Spectroscopy (VERITAS) missions preparing for Venus (Rosenblatt et al., 2021; S. Smrekar et al., 2022; Widemann et al., 2023), Artemis and Commercial Lunar Payload Services (CLPS) preparing for the Moon (Panning et al., 2024; Smith et al., 2020), and BepiColombo on its way to Mercury (Benkhoff et al., 2021). Icy moons are also the focus of upcoming missions, with JUpiter ICy moons Explorer (JUICE) that will ultimately orbit Ganymede (Van Hoolst et al., 2024) and Europa Clipper going to Jupiter's moon Europa (Roberts et al., 2023).

In this planetary exploration framework, we here provide an overview of our current understanding of the crustal structure of the terrestrial planets. We start by providing a discussion on what is the crust and what is known about this geochemical and rheological layer. Next, we summarize the different geophysical approaches to characterize the structure of the crust and present nominal crustal thickness models for the terrestrial planets. Finally, we propose improvements to existing crustal thickness inversion models from both conceptual and theoretical perspectives. In particular, we discuss how the gravity field resolution, data filtering, crustal density as well as the elastic and dynamic support of topography affect crustal thickness models. Although the Earth's crust will not be explicitly discussed, it will be referenced in the context of comparative planetology. For information on the Earth's crust and lithosphere, the reader is referred to Watts (2015) and to Taylor and McLennan (2009) and McLennan (2022) for details on the composition and formation of planetary crusts. Table 1 provides a list of definitions for some specific names used in the geophysics community when discussing the structure of planetary crusts.

2. The Architecture of Planetary Crusts

2.1. What Is the Crust?

The definition of a planet's crust strongly depends on one's field of study. In general, the crust of a planet is understood as being the outermost solid layer with a composition that substantially differs from the deeper interior (mantle and core). The crust is formed and affected by various fractionation processes, and is therefore generally less dense and more enriched in incompatible elements than the mantle. The crust represents a chemical distinction in the layering of a planet interior, in contrast to the lithosphere, which delimits a mechanical distinction.

It is common in planetary science to distinguish between three different types of crust based on how and when the rocks formed (Taylor & McLennan, 2009, Table 1). The *primary crust* is the very first crust to form, resulting from the crystallization of a magma ocean. On the Moon, the felspathic floatation crust that makes up the bulk of the highlands is conventionally defined as a primary crust (McLennan, 2022; Michaut & Neufeld, 2022). The *secondary crust* results from the later partial melting of the mantle. On Mercury, the volcanic smooth plains can be regarded as a secondary crust, as is the case with the lunar maria on the Moon, the vast majority of Venus' crust, or the Tharsis plateau and other volcanic units on Mars. The secondary crust is typically built over long-timescales

BROQUET ET AL. 2 of 28

009139	the same of the first
	and a com a
	a pour against a parties
a magma te grain	Commence of the second
ated mantle	A Comment
Found on ly lower on	CAROLE CROSS SECTION ASSESSMENT
(., Earth's n ⁻³)	second to a second
defined by	Charles or war at a
and where ness or geologic	The second second second
nd location.	the same and a second contract of
relief the relief	Carried to the
elief of a	Contract and
y estimated	of the Course
onal Kaula rule).	to a company of the same
graphy at a y and	a come of account of the contract
et al., 2014; the geolog- lteration or nitic conti- , 2015), but primordial ts the final	agaption of the production of the contract of

Table 1 Nomenclature	
Crust	 Primary crust: The very first crust to form, resulting from the crystallization of a magma ocean (e.g., lunar anorthositic crust). Found on the Moon and Mars. Intermediate grain density (~2,900 kg m⁻³) Primordial crust: The product of the partial melting of a primordial undifferentiated mantle (e.g., Mars' early crust) Secondary crust: The product of mantle partial melting (e.g., lunar mare basalts). Found on all planets. Generally high grain density (~3,300 kg m⁻³), but potentially slightly lower on Mercury (~3,000 kg m⁻³) Tertiary crust: The product of the alternation or partial melting of the crust (e.g., Earth's granitic continents). Found on Earth and Mars. Low grain density (~2,700 kg m⁻³) Icy crust: The outermost ice layer on icy satellites (e.g., Europa's crust)
Lithosphere	 Mechanical lithosphere: The outermost mechanically competent layer of a planet defined by a yield strength criterion. Time-dependent thickness Thermal lithosphere: The outermost cold layer of a planet defined by an isotherm and where heat is transferred by conduction rather than convection. Time-dependent thickness Elastic lithosphere: The outermost layer of a planet that behaves elastically over geologic times. Time-dependent thickness
Free-air Gravity Anomaly	The estimation of the force of attraction of a planetary object at a specific radius and location. Geodesists often call it the gravity disturbance
Bouguer Correction	The estimation of the gravitational attraction (excess/deficit of mass) arising from relief variations at the surface of a planet. <i>Requires an assumption on the density of the relief</i>
Bouguer Anomaly	The estimation of the gravitational attraction due to mass anomalies beneath the relief of a planet. Calculated as Free-Air Anomaly minus Bouguer Correction
Downward/Upward Continuation	The estimation of the gravitational attraction at a radius different from that initially estimated
Gravity Degree Strength	The laterally variable spherical harmonic degree at which the integrated gravitational acceleration uncertainty is above theoretical predictions (often defined from a Kaula rule). Should be used to discard regions with poor gravity field resolution
Admittance	The proportionally constant (or linear transfer function) that relates gravity and topography at a given wavelength. Calculated as the wavelength-dependent ratio of the gravity and topography power spectra

from millions to billions of years. On the Moon and Mars, the secondary crust is basaltic (Baratoux et al., 2014; Kiefer et al., 2012) and was formed by extensive volcanism during the interior evolution and up to the geologically recent past (Hauber et al., 2011; Qian et al., 2021). A *tertiary crust*, resulting from geologic alteration or partial melting of previously formed crust is also often mentioned, particularly on Earth for the granitic continental crust (McLennan, 2022) and sometimes for the highland plateaus on Venus (e.g., Gilmore et al., 2015), but this will not be discussed further. Note that in geochemistry, some authors discuss the existence of a *primordial crust*, which results from the partial melting of a primordial undifferentiated mantle and represents the final product of planetary differentiation (Bouvier et al., 2018). While the primary and primordial crusts are often used synonymously, they differ in composition and petrologic origin. For example, a primordial crust is the result of partial melting and can be basaltic to andesitic in composition (Bouvier et al., 2018), akin to a secondary crust, whereas the primary crust is the result of significant fractional crystallization. A last type of crust, the *icy crust* (or ice shell), is commonly discussed to define the uppermost layer of icy satellites (Nimmo & Pappalardo, 2016) but will not be considered further.

In geophysics, the crust typically refers to the layer ranging from the solid surface to a lower bound defined by a drastic change in material properties. More specifically, in seismology, the base of the crust is identified based on a distinct contrast in seismic velocity (Lognonné & Johnson, 2015), which is related to differences in density and elastic properties (and hence composition and temperature) between the crust and the underneath mantle. Other seismic discontinuities may also be found within the crust that may be linked to intra-crustal layering and porosity (e.g., Durán et al., 2022; Knapmeyer-Endrun et al., 2021; Knapmeyer-Endrun et al., 2025). On Earth, the very first observational constraint on the thickness of the crust was established by Andrija Mohorovičić following an earthquake in 1909 (see English translation in Mohorovičić, 1992). The Earth's crust-mantle interface was later given the name Mohorovičić discontinuity (or often simply *Moho*). It is important to emphasize that the Moho is a

BROQUET ET AL. 3 of 28



seismic discontinuity and is only measured by seismic techniques, which have thus far been applied to the Earth, Moon, and Mars. In geodynamics, the crust is a thermally insulating upper layer characterized by a relatively low thermal conductivity and that is often enriched in heat-producing elements compared to the underneath mantle. On stagnant lid planets, such as Mars or the Moon, the crust is thought to host more than half of the planetary radiogenic element content (Broquet et al., 2025; Laneuville et al., 2018; Plesa et al., 2022). When studying the gravity field of a planet, the base of the crust corresponds to where one observes a large density contrast with the underlying mantle, and that is typically mapped by inverting topography-corrected observed gravity anomalies (hereafter referred to as the Bouguer anomaly). This density contrast often results from a difference in composition between the pyroxenite, andesitic, or basaltic crust and the underneath peridotite or dunite mantle. Importantly, we note that the density of pore-free basalts on the Moon and Mars are similar to the density of the mantle (e.g., Baratoux et al., 2014; Kiefer et al., 2012), and thus, defining the crust solely by density and gravity can be problematic. In this work, we focus on the geophysical definition of the crust in a gravity analysis framework.

2.2. The Density of the Crust

In a geophysical study of the crust using gravity and topography, the bulk density of the crust has a prominent effect on crustal thickness (e.g., Wieczorek et al., 2022). The density of the upper crust affects the Bouguer correction, whereas the density of the lower crust affects the inversion of crust—mantle relief from the Bouguer anomaly (see Table 1 for definitions). It is not expected that the density of the upper crust equals the density of the lower crust due to variations in porosity, composition, and geologic evolution (e.g., Beuthe et al., 2020; Wieczorek & Phillips, 1999). Below, we provide a brief overview on the crustal density of the terrestrial planets.

2.2.1. The Moon

The density and composition of the crust depend on how and when crustal materials are formed. The bulk of the lunar crust is a primary crust predominantly made of anorthosite, a feldspar-rich rock with a grain density of about 2,900 kg m⁻³ (Huang & Wieczorek, 2012; Michaut & Neufeld, 2022; Wood et al., 1970). For comparison, the Earth's granitic continental crust is thought to have a density of about 2,700–2,800 kg m⁻³ (e.g., Mooney et al., 2023). Analyzes of GRAIL data, however, revealed a low bulk crustal density of 2,550 kg m⁻³, which implies a high porosity (~12%, Goossens et al., 2020; Wieczorek et al., 2013). Comparatively, the secondary lunar crust consists of mare basalts, which are iron-rich rocks with higher grain and bulk densities of about 3,300 and 2,850 kg m⁻³, respectively (e.g., Goossens et al., 2020; Kiefer et al., 2012). Mare basalts have higher grain density than typical mid-ocean ridge basalts (or MORB) on Earth due to their enrichment in iron and titanium (McLennan, 2022). Importantly, the secondary crust of the Moon is thought to only represent a minor ~1% volume fraction of the total crust volume, though this quantity varies substantially with regional values reaching 50% in mare-covered basins (Broquet & Andrews-Hanna, 2024b). Some studies have also mapped high-density intrusions throughout the lunar surface (e.g., Jozwiak et al., 2012; Kiefer, 2013; Thorey et al., 2015), but these generally also represent a ~1% volume minor fraction of the crust (Broquet & Andrews-Hanna, 2024b).

In addition to lateral variations in composition, which are often observable at the surface, the crust of the Moon and other planets can be stratified. The uppermost tens to hundreds of meters of the crust is typically referred to as the regolith and is made of unconsolidated rock materials caused by repeated small-scale impact events (e.g., Fa & Wieczorek, 2012; McKay et al., 1991). Directly below the regolith likely lies a heavily fractured upper crust, referred to as the megaregolith that is a result of in situ fracturing of the crust by large-scale impact events or thick ejecta deposits from impact basins (McKay et al., 1991; Rodriguez et al., 2020; Wiggins et al., 2022). These two layers have high porosity and low density. Although the detailed characteristics of the megaregolith remain challenging to constrain, the presence of this layer can have profound geophysical implications for the planetary body. For example, a megaregolith can affect seismic-wave propagation and thermally insulate the crust (Warren & Rasmussen, 1987). A gravitation signal can also be induced by relief across a porous units and more intact materials underneath (e.g., Venkatadri & James, 2020), which can affect crustal thickness inversions from gravity and topography. On the Moon, inversion of gravity and topography data suggest an increase in crustal density with depth by a few tens of kg m⁻³ per kilometer (Besserer et al., 2014; Goossens et al., 2020), which is likely related to a porosity decrease with depths due to overburden pressure and viscous closure of pores (Han et al., 2014; Wieczorek et al., 2013). In contrast, in the mare regions, gravity data show evidence for high density basalts overlying less dense highland materials (Besserer et al., 2014; Gong & Wieczorek, 2016).

BROOUET ET AL. 4 of 28

2.2.2. Mars

On Mars, analyzes of orbital gamma ray spectrometer data indicated the planet to be a basalt-covered world, hosting a thick secondary basaltic crust with grain densities ranging from 3,250 to 3,450 kg m⁻³, higher than that found on Earth (Baratoux et al., 2014). As for the Moon, these intrinsically high grain densities are a result of a high FeO content. The porosity and hence the bulk density of this secondary crust, however, remains challenging to constrain. It is generally thought that bulk porosity on Mars should be lower than on the Moon (~12%) due to the former likely having higher thermal gradients that would allow for viscous closure of porosity at depths shallower than on the Moon (Gyalay et al., 2020). Additionally, the infill of pore space by ice, water, or aqueous alteration products would decrease the overall bulk porosity of the Martian crust compared to the Moon. Interestingly, having a predominantly basaltic crust on Mars is inconsistent with the relatively low bulk densities inferred from seismic and gravity data (<3,100 kg m⁻³, Wieczorek et al., 2022) as well as from localized admittance studies (~2,600 kg m⁻³, Goossens et al., 2017; see Section 2.3.5 and Table 1 for more information on the admittance approach). Although one can argue that a localized admittance analysis is only sensitive to the density of the uppermost crust (compared to a crustal thickness inversion that is sensitive to the density of both the upper and lower crust), this suggests the widespread existence of a lower density, likely more felsic and potentially primary crust (see Bonnet Gibet et al., 2025; Wieczorek et al., 2022).

In situ analyzes also support the existence of low-density crustal rocks on Mars. Based on Mars Pathfinder data, Neumann et al. (2004) estimated the density of some pore-free rocks to be \sim 3,060 kg m⁻³, which is substantially lower than typical Martian basalts. Within the Gale crater, silica- and feldspar-rich rocks have also been observed by the rover Curiosity, suggesting the presence of a low-density continental-like crust (Sautter et al., 2015). Lewis et al. (2019) estimated the grain density of the surface material within Gale crater to be about 2,800 kg m⁻³, and using the onboard accelerometers, the authors constrained the subsurface sedimentary rock bulk density, representative of the 300 m thick section traversed by Curiosity, to be 1,680 kg m⁻³. The difference between these two estimates can be explained by a large unfilled porosity (or void space) of about 40%. The Medusa Fossae formation, located at the equator near Elysium Planitia, also hosts thick low density, \sim 1,765 kg m⁻³, and highly porous dusty materials (Ojha & Lewis, 2018). Finally, the Martian poles harbor thick ice caps of low density, <1,500 kg m⁻³, that are dominantly made of water ice (Broquet et al., 2020, 2021; Genova et al., 2024; Wieczorek, 2008; Zuber et al., 2007). All these units as well as the possible existence of a low-density lower crust will affect estimates of Mars' crustal thickness (Wieczorek et al., 2022).

2.2.3. Mercury and Venus

The bulk density of the crusts of Mercury and Venus remains poorly constrained. Due to the low-resolution of the gravity field on both planets, it is challenging to uniquely constrain the crustal density using these data sets.

On Mercury, analyzes of orbital gamma ray spectrometer data also suggest the presence of a high-density crust, though less dense than the secondary crust of Mars or the Moon, with values of about 2,950 kg m $^{-3}$ (Beuthe et al., 2020). Similar densities were also found using normative mineralogy and the X-ray spectrometer onboard MErcury Surface, Space ENvironment, GEochemistry, and Ranging (MESSENGER, Sori, 2018). Interestingly, only moderate differences in grain density ($\pm 100~{\rm kg~m}^{-3}$) were found between the planet's smooth plains and surrounding cratered terrain. One region with a high Mg surface composition, however, stood out with estimated grain densities of $\sim 3,100~{\rm kg~m}^{-3}$. Localized admittance analyzes by Genova et al. (2023) reported bulk densities of 2,540 kg m $^{-3}$ in a few analyzed regions, which only cover 8% of the planet's surface and are all located near the north pole, indicating substantial crustal porosity comparable to the Moon ($\sim 15\%$). However, as discussed above, the depth-sensitivity of localized admittance investigations remains unclear, and the inferred bulk density might only be representative of the upper crust. Analyzes based on the planet's basin and crater populations also reported generally high and lunar-like porosities for Mercury's crust (Broquet et al., 2024).

X-ray fluorescence measurements from Soviet landers in the 1980s indicated Venus' surface to be primarily basaltic, with a composition similar to tholeitic basalts found in Earth's oceanic crust (Surkov et al., 1984, 1986). Tholeitic basalts typically have grain densities ranging from about 2,900 to 3,000 kg m⁻³ (Stolper & Walker, 1980). However, because the porosity and deeper composition of Venus' crust are largely unknown, the bulk density of the planet's crust remains challenging to estimate. Venus has relatively few impact craters, and erosional processes are likely weak due to the absence of water and low surface winds in the geologically recent past. Hence, the planet may lack a thick high-porosity regolith layer. Deeper pore space (>10 km) would also be

BROQUET ET AL. 5 of 28

more susceptible to viscous closure due to the higher temperatures on Venus compared to the other terrestrial planets. On the other hand, several studies suggest that explosive volcanism and pyroclastic flows are widespread on Venus (e.g., Campbell et al., 2017; Ganesh et al., 2021), which could contribute to at least locally high crustal porosities. Localized admittance analyzes are generally only weakly sensitive to crustal density at the wavelengths resolved by current Venusian gravity models (e.g., Maia & Wieczorek, 2022).

Together, these analyzes indicate that primary crusts typically have low densities, comparable to the Earth's continental crust, while secondary basaltic crusts have higher densities. The density difference results from composition but can also be increased by porosity differences. The secondary crust typically sits on top of the primary crust but can also be found in abundance intruding into the primary crust (e.g., White et al., 2006). Although this layering can have a drastic effect on crustal thickness models (e.g., Broquet & Andrews-Hanna, 2024a), the relative contribution of each layer to the gravity field is challenging to estimate. Density variations with depth, due to porosity or composition, are also expected within planetary crusts. A density increase with depth can be explained by a decrease in porosity due to the higher temperature and pressure at greater depth, but can also be linked to changes in composition. As further discussed below, on large planets like Venus or Earth, the basalt-eclogite transition can be achieved within the crust, thereby substantially increasing the density of the lower crust.

2.3. Constraints on Crustal Density and Thickness From Gravity and Topography Analyzes

2.3.1. Classical Inversions of Gravity and Topography for Crustal Thickness

Inversions of potential fields are inherently non-unique. Joint analyzes of gravity and topography data are no exception and cannot uniquely determine the interior structure of a planet, including the thickness of its crust. A non-linear inverse approach can be used to predict the shape of the crust-mantle relief that depends on the assumed crust and mantle density, but it cannot determine the mean radius at which the relief occurs. For that reason, the average radius of the crust-mantle interface needs to be fixed a priori, which implies that gravity and topography inversions alone cannot provide absolute estimates of crustal thickness (e.g., Wieczorek & Zuber, 2004). In addition, such inversions cannot determine whether interior gravity anomalies arise from differences in crustal density or thickness, thereby requiring additional assumptions. For example, by assuming the crust to be in an isostatic state (i.e., a mass, pressure or stress equilibrium in the crust, see Hemingway & Matsuyama, 2017), a hypothesis which is often challenging to evaluate, one can estimate absolute crustal thicknesses (e.g., Padovan et al., 2015; Wieczorek & Zuber, 2004). In its simplest Cartesian form, this estimate solely depends on the planet's topography and the assumed densities of the crust and mantle. Importantly, while the primary crust of a planet is expected—and has been argued (e.g., Padovan et al., 2015; Sori, 2018)—to initially form in a state of isostasy, such as a floatation crust on the Moon (e.g., Broquet & Andrews-Hanna, 2024a), later modifications of the crust by volcanism or impacts would potentially induce strong departure from isostasy. Thus, the assumption of isostasy must be limited to specific regions or wavelengths of interest (e.g., Padovan et al., 2015).

In the sections below, a *classical crustal thickness inversion* refers to the approach detailed in Wieczorek et al. (2022) (see also Bills & Ferrari, 1977; Neumann et al., 1996, Wieczorek & Phillips, 1998), which ascribes Bouguer anomalies to relief at the crust–mantle interface without assumptions regarding the support mechanism (i.e., elastic flexure, Airy or Pratt isostasy). The approach can be summarized as follows (see Table 1 for definitions):

- 1. The *Bouguer correction* is estimated assuming a crustal density, in order to remove the gravity contribution from the known surface topography to the observed gravity field. Methods to estimate the gravity anomaly from finite-amplitude relief on a spherical planet are discussed in Wieczorek and Phillips (1998).
- 2. The Bouguer correction is removed from the observed free-air gravity in order to obtain the *Bouguer anomaly*.
- 3. The Bouguer anomaly is *downward continued* from the reference radius at which it was computed (often the mean planetary radius or spacecraft altitude) to the assumed mean radius of the crust–mantle interface. This approach corrects for the gravity decrease with distance, which amplifies short-wavelength power. When high degrees are subject to noise in the data, a low-pass filter is applied (see Neumann et al., 1996; Wieczorek & Phillips, 1998). More information on this filtering process is given below.

BROOUET ET AL. 6 of 28

assumption of a specified density contrast across this interface.

This general approach has been developed over many years (e.g., Bills & Ferrari, 1977; Neumann et al., 1996; Phillips & Lambeck, 1980; Wieczorek & Phillips, 1998) and requires three main assumptions: (a) the density of the surface topography; (b) the average thickness of the crust; (c) the density contrast across the crust–mantle interface. Additional steps can be incorporated to account for other interior mass anomalies arising from the mantle and core or low-density surface units, and lateral variations in crustal density, are discussed in Wieczorek et al. (2022) and in the sections below. Several codes to solve for crustal thickness using the above approach exist,

2.3.2. Classical Crustal Thickness Inversion Under a Minimum-Thickness Constraint

including ctplanet (Wieczorek, 2024) and Displacement-Strain-Planet (DSP, Broquet, 2024a).

For Mercury and Venus (but also for the Moon and Mars), our knowledge of the detailed structure of the crust primarily relies on non-unique gravity and topography inversions. External assumptions can however be supplied to alleviate the non-uniqueness. One simple physical constraint is that crustal thickness must be everywhere greater than zero. Under such considerations, a lower bound on the average thickness of the crust can be given together with an upper bound on the density of the crust (see also Wieczorek et al., 2022). This can be understood as follows: As the crustal density increases, the density contrast across the crust-mantle interface decreases. To maintain the same gravity anomaly with a relatively higher crustal density, it is necessary to compensate for the smaller density contrast with larger lateral variations of the crust-mantle relief. These large oscillations of the crust-mantle relief will make the modeled crust mantle interface go above the surface, resulting in an unphysical situation where the crustal thickness is negative. Thus, for one given crustal density, it is possible to estimate the minimum average crustal thickness. Importantly, we note that this approach is sensitive to the density of the crust in regions where near-zero crustal thickness is retrieved, and these are often found within large impact basins. If such regions have a density different from the rest of the planet, as a result of the impact melt sheet, extrusive lavas, sedimentary deposits, crustal porosity, or intrusive activity (e.g., Freed et al., 2014), the retrieved crustal properties might not adequately reflect the planet's crustal structure.

Here, we use this minimum-thickness approach to provide constraints on the thickness of planetary crusts. For each planet, we estimate the end-member crust and mantle properties required to have non-zero crustal thickness globally. This provides us with a minimum average crustal thickness and associated maximum crustal density. Higher crustal density can be obtained if the average crustal thickness is increased. The gravity and topography data used for this model are described in Table 2. Considering a set of crust and mantle densities of 2,800 and 3,300 kg m⁻³, somewhat similar to Earth and as typically used in the literature (e.g., James et al., 2013), our model indicates minimum average crustal thicknesses of 18 and 10 km for Mercury and Venus, respectively (Figures 1a and 1b). Interestingly, these values are substantially lower than for Mars or the Moon, which have minimum crustal thicknesses of about 50-55 km for similar interior densities (Figures 1c and 1d). Comparatively, Mars and the Moon generally have more pronounced gravity anomalies (Figure S1 in Supporting Information S1) and also host large and deep impact basins that quickly reach a zero crustal thickness as crustal density increases. Our minimum-thickness analysis allows for the possibility that Mars and the Moon could have thicker crusts than Mercury and Venus. For the Moon and Mars, our analysis also indicates that the density contrast between the crust and mantle cannot be lower than 500 and 400 kg m⁻³, respectively, while such models are allowed on Venus and Mercury. Again, this is compatible with the possibility that Mars and the Moon have could low-density crusts (or high-density mantle) when compared to Mercury and Venus. Such a density difference may be related to the specific evolution of Mercury and Venus, as both planets are thought to have lost a large fraction of their primary crusts (Armann & Tackley, 2012; Marchi et al., 2013).

To complement these minimum crustal thickness models, upper bounds on the thickness of the crust can be given based on geochemical and/or geodynamical arguments. For example, an overly thick crust may be incompatible with either the bulk composition of the planet (Taylor et al., 2006; Taylor & Wieczorek, 2014; Wieczorek & Zuber, 2004) or the depth at which the crust is expected to viscously relax (>100 km; Wieczorek et al., 2022; Nimmo & Mackwell, 2023). In addition, in the case of an overly thick crust, the basalt-eclogite transition may appear in the lower crust. Because eclogite is thought to have a bulk density similar to the underneath mantle (Ito & Kennedy, 1971), crustal materials deeper than the eclogite–mantle interface will be mostly unseen in gravity

BROOUET ET AL. 7 of 28

	Mercury	Venus	The Moon	Mars
Planetary shape	DEM ^a Resolution: Good (~5 km)	VenusTopo719 ^b Resolution: Good (~50 km)	LOLA ^c Resolution: Great (<1 km)	MOLA ^d Resolution: Great (<1 km)
Expected improvements	BELA ^e	VISAR, VEM & VenSAR ^{f,g}	-	-
Planetary gravity field	<i>HgMM09</i> ^h Resolution: Low & Variable (∼170–1,400 km)	MGNP180U ⁱ Resolution: Low & Variable (~400–1,000 km)	GRGM1200B ^j Resolution: Great (∼20 km)	GMM3 ^k Resolution: Good enough (~230 km)
Expected improvements	MORE ¹ (~170–340 km)	VERITAS Gravity Science & EnVision RSE ^{f,g} (~200 km)	-	-
Absolute crustal thickness, km	Unknown	Unknown	31–38 (±8) at Apollo landing sites ^m	39 ± 8 at InSight's landing site ⁿ
Additional considerations	26 ± 11 globally, assuming Airy isostasy°	20 globally, assuming Airy isostasy ^p	Near-zero at basins with mantle ejecta. Farside seismic constraint? ^q	
Average crustal thickness, km (nominal)	>10 [*] (35)	>4 [*] (15)	34–43 ^r (40)	30–72 ^s (57)
Total mass, ×10 ²² kg (nominal)	>0.2 (0.7)	>0.5 (1.9)	0.3-0.4 (0.4)	1.2–3.1 (2.5)
Silicate mass fraction % (nominal)	>2.5 (9.3)	>0.2 (0.8)	5.1-6.5 (6.0)	2.5–6.4 (5.6)

Note. A rough estimate of the horizontal resolution of each data set is given in parentheses. The comment on the data quality is given in the context of a crustal thickness inversion for which the gravity field resolution is always the limiting factor. The gravity field resolution corresponds to the full wavelength using Jeans relation, $\lambda \approx 2\pi R/\sqrt{L(L+1)}$, where R is the planetary radius and L the maximum resolved spherical harmonic degree. *Minimum average crustal thickness for constant crust and mantle densities (Figure 1). Silicate mass fractions are given assuming core sizes of 2,000, 3,500, 380 and 1,830 km for Mercury, Venus, the Moon and Mars, respectively (Breuer & Moore, 2015). Acronyms include: Digital Elevation Model (DEM), Lunar Orbiter Laser Altimeter (LOLA), Mars Orbiter Laser Altimeter (MOLA), BepiColombo Laser Altimeter (BELA), Mercury Orbiter Radio-Science Experiment (MORE), Venus Interferometric Synthetic Aperture Radar (VISAR), Venus Emissivity Mapper (VEM), Venus Synthetic Aperture Radar (VenSAR), Radio Science Experiment (RSE). *Becker et al. (2016). *Wieczorek (2015). *Smith et al. (2010). *Gmith et al. (2001). *Thomas et al. (2021). *Rosenblatt et al. (2021). *S. Smrekar et al. (2022). *Genova et al. (2023). *Konopliv et al. (1999). *Goossens et al. (2020). *Genova et al. (2016). *Iess et al. (2021). *Wieczorek et al. (2022). *Wieczorek et al. (2022). *Wieczorek et al. (2023). *Wieczorek et al.

data. However, given the large density contrast of the upper-crust–eclogite interface, this layer will mimic the gravitational signal of a typical crust–mantle interface. Therefore, in the context of gravity and topography inversion, the top of the eclogite layer will generally appear as the base of the crust. Depending on the interior temperature and rheology, the eclogite layer can sink into the mantle and delaminate. If delamination is expected, the thickness of the planet's crust can be limited by the basalt–eclogite transition.

For Venus, the basalt–eclogite transition is thought to occur around 50 km, thought this depends on poorly known thermodynamic parameters and the variable planetary heat flow (Hess & Head, 1990; Maia & Wieczorek, 2022). Nevertheless, if one adds the constraint that the Venusian crust cannot be thicker than 50 km anywhere on the planet, the average crustal thickness becomes to 8–10 km for a crustal density of 2,700 kg m⁻³, with the upper bound being limited by eclogitization (see also James et al., 2013). At fixed temperature, Mercury's lower gravitational attraction and pressure in the crust would make eclogitization substantially deeper (about 2.5 times), making this constraint rather weak (inferred maximum crustal thicknesses >100 km). Similar effects would also make the basalt-eclogite transition occur deep in the Martian interior, with experiments suggesting depths of ~250 km and with eclogite materials having density comparable to the ambient mantle (Zhou et al., 2022), although different depths could be obtained considering different mantle compositions. In addition, Mars' colder interior and thicker lithosphere would likely hinder most geologically recent subcrustal dynamics (Plesa et al., 2018). Thus, while the lower crust of Venus may be subject to eclogitization and Earth-like delamination, this would generally not be the case on other smaller and colder worlds.

The non-uniqueness in gravity modeling can also be resolved when absolute measurements or absolute estimates of crustal thickness exist. On the Moon, olivine exposures in the vicinity of large basins, such as Crisium and Moscoviense, are consistent with the excavation of mantle materials, which would imply near-zero crustal

BROQUET ET AL. 8 of 28

21699100, 2025, 9, Downloaded from https://agupubs.onlinelibrary.wiley.

com/doi/10.1029/2025/E009139 by Disch Zentrum F. Luft-U. Raum Fahrt In D. Helmholtz Gemein., Wiley Online Library on [07/10/2025]. See the

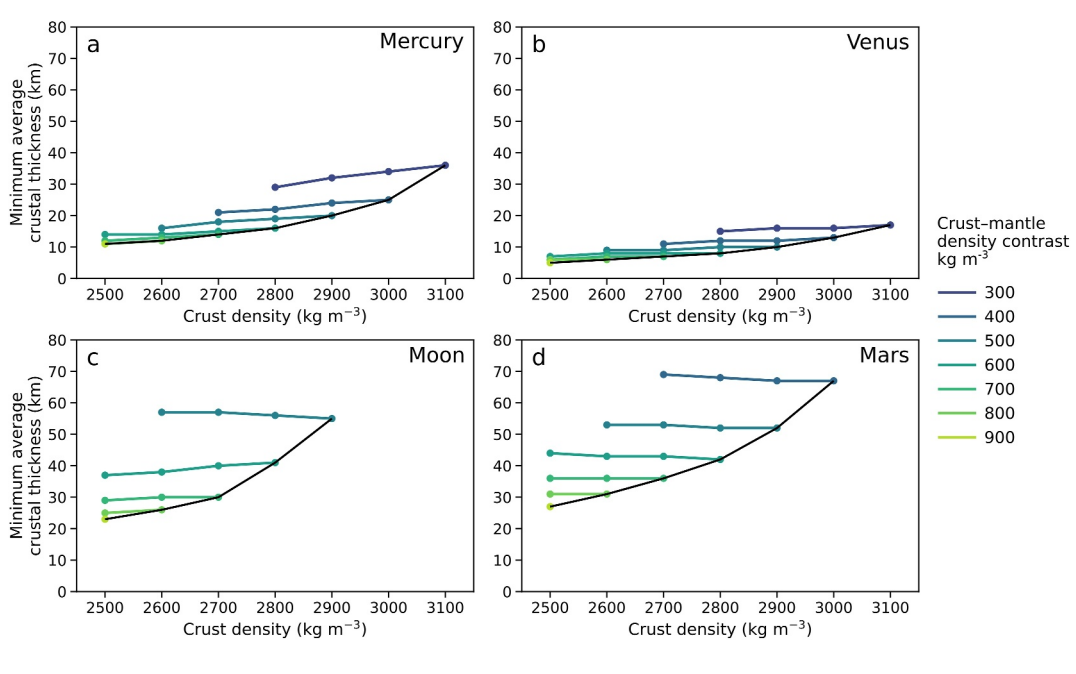


Figure 1. Minimum average crustal thicknesses for Mercury (a), Venus (b), the Moon (c) and Mars (d) as a function of crustal density and crust—mantle density contrasts. The investigated crustal and mantle densities range from 2,500 to 3,200 kg m⁻³ and 3,100 to 3,500 kg m⁻³, respectively. Regions below the black lines lead to implausible crustal thickness models (negative crustal thicknesses or not converging).

thickness within the basin interior (Wieczorek et al., 2013; Yamamoto et al., 2010). Although the exact value of near-zero thickness could range from a few hundred meters to several kilometers, this external constraint can be used to limit a crustal thickness inversion and obtain absolute crustal thickness estimates. Alternatively, using seismically derived measurements of crustal thickness, it is possible to fully constrain a crustal thickness model as done on the Moon (Wieczorek et al., 2013) and on Mars (Wieczorek et al., 2022). Absolute crustal thicknesses are obtained by exploring a large range of mean crustal thicknesses, and crustal and mantle densities to find the models that best fit the seismic measurements. In this way, a locally measured crustal thickness can be extrapolated to the entire planet. Importantly, as with the minimum-thickness models discussed above, this extrapolation depends on how the crustal density in the region where crustal thickness was estimated or measured compares to the planet's global properties.

2.3.3. Inversions of Gravity and Topography With Dynamic Flow in the Mantle

Some previous studies have performed two-layered inversions of observed gravity and topography data considering dynamic mantle flows, which are appropriate when mantle buoyancy is expected to provide support to topographic loads, such as on Venus (e.g., Herrick & Phillips, 1992; James et al., 2013) or Mercury (James et al., 2015). Therein, the two free parameters are generally the crust—mantle interface relief and mantle density, and the constraints are observed gravity and topography. These two-layered inversions assume either no lithospheric strength, in which case the topographic loads are compensated by the radial normal stress associated with buoyant crustal roots and dynamic flows in the mantle, or a lithosphere that resists the displacement associated with dynamic topography. Such models need an assumed input viscosity structure for the mantle, with no lateral variations, and solve for mantle flow using a propagator matrix approach (e.g., Richards & Hager, 1984). The dynamic flow model differs from the inversion presented and developed below in which mantle buoyancy is resisted by an elastic lithosphere. Importantly, the contribution of the mantle to the gravity field is generally most important for the longest wavelengths due to the depth-attenuation of gravity anomalies. Thus, considering mantle flow will mostly affect the long-wavelength structure of the crust.

BROOUET ET AL. 9 of 28

2.3.4. A Matrix Inversion of Gravity and Topography

Gravity and topography can also be inverted using a system of equations that accounts for lithospheric flexure (Banerdt, 1986). In this approach, a system links the topography, geoid (or gravity), net load acting on the lithosphere, tangential load potential, flexure of the lithosphere, crustal root variations and density variations. Given three constraints or assumptions, the system can be evenly determined. This model was adapted by Broquet and Andrews-Hanna (2023a) to account for a finite-amplitude correction when computing gravity. The relief across different interfaces is iteratively solved using parameters similar to the classical model described above (i.e., average density of the crust and mantle, and average crustal thickness) with the addition of the elastic thickness of the lithosphere. This latter parameter is inversely proportional to the rigidity of the lithosphere and controls the amount of lithospheric deformation. To reproduce a classical crustal thickness model, the three specified constraints/assumptions to solve this model are (a) the observed topography, (b) the observed gravity, and (c) the assumption that there are no lateral density variations.

One advantage of this model is its versatility and its usefulness beyond crustal thickness modeling. For example, the interior structure of a planet could be solved in a flexural–Pratt compensation regime, for which all is needed is to assume that there are no crustal root variations (aside from flexure), in addition to using observed gravity and topography (i.e., 3 constraints/assumptions). Alternatively, the model can predict the topographic and gravitational signature of a mantle plume by assuming that the input mantle density variations, representing the plume, are compensated by dynamic topography only (i.e., 3 constraints/assumptions; mantle density, no crustal root, and plume-induced topography equals flexure, see Broquet & Andrews-Hanna, 2023a). Compared to a classical crustal thickness inversion, this model is also able to extract a flexural displacement component from the relief at the crust–mantle interface, pending an assumption on the elastic thickness of the lithosphere. The vertical and tangential displacements can then be used to infer crustal strains that can be compared to the tectonic record (e.g., Broquet & Andrews-Hanna, 2023b). In this work, we make use of the Displacement-Strain-Planet (DSP) code that solves this matrix inversion, for which a documented open-source package is available at Broquet et al. (2024). While this package currently only works with a globally constant elastic thickness, which may not adequately capture the complexity of a time-integrated loading history, future work will be implemented to resolve this issue.

2.3.5. Forward Modeling of Gravity and Topography

An alternative approach to inverting observed gravity and topography is to use a geophysical model of the interior to predict either of these quantities. Because the topography of a planet is generally better known than the gravity field, previous models have typically used the observed planetary shape together with a transfer function, modeling the interior response to loading, to predict the gravity field (e.g., Phillips & Lambeck, 1980). In the spectral domain, this wavelength-dependent transfer function is referred to as the *admittance*, and requires assumptions regarding the density, thickness, and rigidity (or viscosity) of the different interior layers (e.g., Broquet & Wieczorek, 2019; Turcotte et al., 1981, Table 1). In general, an admittance analyzes investigates a large parameter space to forward model the gravity field, and the difference between the model and observations is used to infer best-fitting parameters and shed light on the interior structure of the planet. Being a forward model, this approach naturally differs from the inversions described above, with the downside that it will never fully describe observations. One advantage of the admittance model, however, is to be able to focus on specific regions that are affected by unique geodynamic processes using a spatio-spectral localization technique (see e.g., McGovern et al., 2002; Wieczorek & Simons, 2005). By comparing the modeled and observed admittances, one can estimate the best-fitting interior properties of the region of interest.

In the spatial domain, some studies have also analyzed the geoid-to-topography ratio (or GTR, e.g., Kucinskas & Turcotte, 1994; Wieczorek & Zuber, 2004). The GTR provides a single number that describes the linear relationship between geoid and topography. Compared to a localized admittance analysis, this approach preserves spatial information at the expense of squashing all wavelengths into a single number. Thus, inferring the relative influence of different input parameters or from wavelengths larger than the study region can be difficult (Wieczorek & Zuber, 2004). Under the assumption of Airy isostasy, however, a GTR approach can constrain the average crustal thickness of a region and this approach was widely used in early Venus and Mars science (e.g., S. E. Smrekar & Phillips, 1991; Turcotte et al., 2002).

BROOUET ET AL. 10 of 28

2.3.6. Inversions for the 3-D Crustal Structure

Additional inversion approaches have been developed to probe the 3-D interior structure of a planet using gravity and topography data. While primarily applied to Earth (Li & Oldenburg, 1998), 3-D inversions have sparked interest in lunar science following the GRAIL mission (e.g., Jansen et al., 2017; Liang et al., 2014). These 3-D inversions generally discretize the interior into tesseroids or some other shape for which a gravitational field can be effectively computed (Uieda et al., 2016). For example, Zhao et al. (2019) subdivided the lunar interior into tesseroids to invert the Moon's interior structure under some normalization constraints. Synthetic tests and comparison with classical models demonstrated the applicability of a 3-D inversion of GRAIL data to retrieve the shape of the crust—mantle interface as well as density anomalies in the crust and mantle. Other notable studies include the work of Geng et al. (2024), which constrained the magmatic plumbing system in the Oceanus Procellarum region on the Moon, and Mittelholz et al. (2025) that proposed a joint inversion of gravity and magnetic data in the southern hemisphere of Mars. Importantly, the simulated gravity field strongly depends on an assumed depth-weighting function that distributes density anomalies with depth.

Inversions for the 3-D interior structure of a planet using shape models can also be useful when the gravity field is unevenly known. On the Moon, Hikida & Wieczorek (2007) used polyhedral shape models to constrain crustal thickness based on pre-Kaguya gravity models that had extremely poor resolution on the farside (Namiki et al., 2009). This approach allowed obtaining a crustal thickness model that better represented the data available at the time, though at the expense of a slow computation time as well as additional input parameters, including the distance between vertices. Importantly, while these approaches can provide useful information on the interior structure of a planet, they remain subject to the inherent non-uniqueness of potential field inversion, as is the case for all models investigating gravity data.

2.4. Nominal Crustal Thickness Models of the Terrestrial Planets

In this section, we present nominal crustal thickness models, starting with Apollo-constrained lunar crustal thicknesses and followed by the InSight-derived crustal thickness of Mars. We finish with Venus and Mercury, whose crustal structures are substantially less constrained. Gravity and topography data used for these models are described in Table 2. These models were constructed using our DSP code with some improvements from both a conceptual and theoretical perspectives. We emphasize that these improved considerations do not substantially affect crustal thickness models, such that the nominal crustal thicknesses presented below are not too different from existing models. For that reason, we here present our nominal models and relegate the detailed discussion on our improved considerations to the following sections.

2.4.1. The Moon

On the Moon, data from the seismic network deployed at the Apollo 12 and 14 landing sites (as well as from Apollo 15 and 16) indicated best-fit average crustal thicknesses of 30 ± 2.5 km (Lognonné et al., 2003) or 38 ± 3 km (Khan & Mosegaard, 2002) for the region encompassing all four Apollo stations, though most of the data came from Apollo 12 and 14. Crustal thickness was also constrained at other locales, including artificial impact locations away from the Apollo network, although with a higher uncertainty (Chenet et al., 2006). Together with GRAIL data, which allowed constraining a low average crustal density for the lunar highlands, the thickness of the crust was found to range from 34 to 43 km. Accounting for the uncertainty in the seismically derived Apollo crustal thicknesses, this range would increase by ±10 km. A model considering the higher density of the mare obtained similar average crustal thicknesses but highlighted major thickness differences in marecovered regions (Broquet & Andrews-Hanna, 2024a). Important limitations to these models include our imperfect knowledge of the depth and spatial variation in crustal and mantle composition and porosity, which are difficult to uniquely infer (see Goossens et al., 2020; Huang et al., 2022; Wahl et al., 2020; Šprlák et al., 2020). These models are further anchored using seismic crustal thickness measurements made on the nearside, which may have different properties than the farside. We note, however, that the zero crustal thickness constraint, which occurs beneath Moscoviense and Crisium, does provide information on the lunar crust far from the Apollo stations. Future seismic constraints on crustal thickness in the farside would contribute to resolving this important issue (Panning et al., 2024).

Our nominal crustal thickness model for the Moon assumes a highland crustal density of 2,550 kg m $^{-3}$, a mare density of 2,850 kg m $^{-3}$, a mantle density of 3,220 kg m $^{-3}$, and an average thickness of 40 km and is described in

BROOUET ET AL. 11 of 28

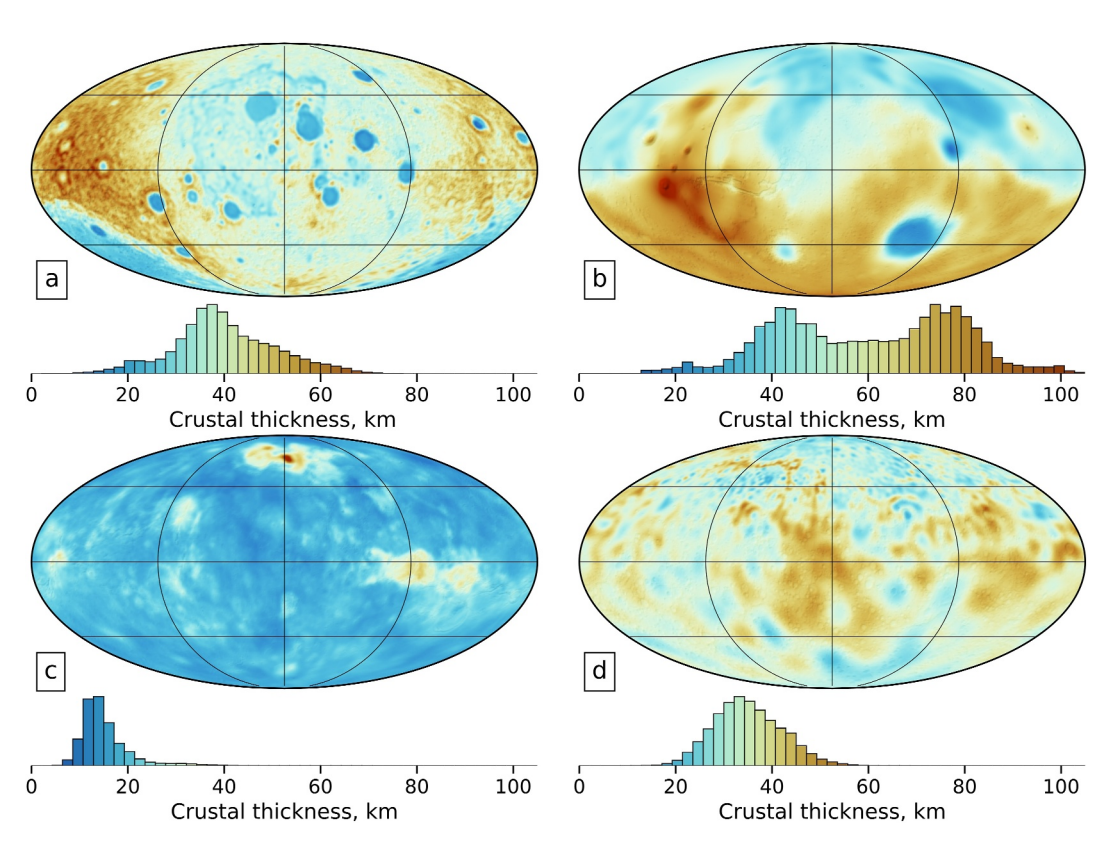


Figure 2. Nominal crustal thickness models for the Moon (a), Mars (b), Venus (c), and Mercury (d). All models are presented in a Mollweide projection centered on 180°E. Color-coded histograms of the area-weighted crustal thickness are shown below each plot.

Broquet and Andrews-Hanna (2024a). For this model, the thickness of the lunar crust ranges from about 30 km in the nearside Procellarum region to 70 km in the farside highlands, and is 33–35 km at the Apollo 12 and 14 landing sites (Figure 2a). In this model, the crust represents 6% of the silicate mass fraction of the planet, which is substantially higher than that on Earth (0.8%).

2.4.2. Mars

On Mars, analyzes of InSight seismic data by Knapmeyer-Endrun et al. (2021) indicated the presence of three crustal discontinuities, two of which could be related to the base of the crust (see also Durán et al., 2022). For a summary of pre-InSight considerations on Martian crustal thickness, we refer the reader to Wieczorek and Zuber (2004). One of these two discontinuities was at a depth of 20 ± 5 km, while the other was at a depth of 39 ± 8 km. The shallowest seismic discontinuity was found at 10 km depth and is likely due to intra-crustal layering rather than the base of the crust. Using the preferred deeper crust-mantle interface at the InSight location, the average crustal thickness was found to lie between 30 and 72 km with a maximum bulk density of 3,100 kg m⁻³ (Wieczorek et al., 2022). Analyzes using additional seismic constraints away from the landing site later suggested the crust to be 42–56 km thick on average (Kim et al., 2023, see also Li et al., 2022), and that the 20 km interface at InSight could be related to porosity or volcanic flows, amongst other factors, rather than the crust-mantle boundary (Kim et al., 2021). Geodynamic models of Mars also typically favor large crustal thickness models in order to fit various geophysical observations, including flexure at the poles and geologically recent volcanism (e.g., Broquet et al., 2025; Plesa et al., 2022). Compared to the Moon, this larger range of plausible average crustal thicknesses results from both the uncertainty in the seismic crustal thickness and our relatively poor knowledge of the bulk density of the Martian crust, with studies suggesting low lunar-like densities (Goossens et al., 2017) or higher basaltic-like densities (Baratoux et al., 2014). One further unknown is whether density differences between Mars' northern lowlands and southern highlands exist (see Bonnet Gibet et al., 2025; Wieczorek et al., 2022).

BROQUET ET AL. 12 of 28

Our nominal Martian crustal thickness model assumes a bulk crustal density of 2,900 kg m⁻³ and a mean thickness of 60 km, together with an upper mantle density of 3,382 kg m⁻³ (Wieczorek et al., 2022). In this model, we assume that short-wavelength gravity anomalies partially originate from crustal density variations extending from the surface to the base of the crust. As further described in Section 3, this approach improves classical models that filter out and discard a portion of short-wavelength data. Note that this model doesn't account for the low-density north and south polar caps, which moderately affect crustal thickness by a few kilometers (Wieczorek et al., 2022). Crustal thickness is found to range from about 40 km in the northern lowlands to 75 km in the southern highlands, reaching 100 km in the Tharsis plateau, and is 40 km at the InSight landing site (Figure 2b). In this model, the crust represents 6% of the silicate mass fraction of the planet, which is similar to the Moon but higher than Earth.

2.4.3. Venus

Compared to other planets, the thickness of the Venusian crust is poorly known. Notable constraints on the crustal structure originate from inversions of spatio-spectrally localized gravity and topography data. One study by Anderson and Smrekar (2006) provided a global map of crustal and lithospheric thickness using a localized admittance approach, with crustal thickness values of about ~20 km and as high as 100 km. Work by James et al. (2013) discussed the possibility for long-wavelength mantle support of the topography and suggested planetary average crustal thicknesses of 8–25 km, where the lower limit is based on the non-zero crustal thickness constraint and the upper bound is based on an assumed depth of the basalt-eclogite transition. A study by Maia and Wieczorek (2022) indicates that crustal plateaus are close to being isostatically supported and imply global average crustal thicknesses of about 20 km, with thicknesses around 30–40 km within the crustal plateaus. However, as discussed above, these models are largely non-unique and suffer from our relatively poor knowledge of the Venusian gravity field, both of which make absolute estimates of any parameter relatively uncertain.

Our nominal model considers the effect of the laterally variable resolution of Venus' gravity field, which is prominent on this planet (see Section 3 below), and assumes an average crustal thickness of 15 km and constant density of 2,700 kg m⁻³, with a mantle density of 3,200 kg m⁻³. For this model, the thickness of the crust is ~35 km within the crustal plateaus, such as Ovda Regio or Ishtar Terra (~45 km at Maxwell Montes), but is drastically lower elsewhere with values of 10 km (Figure 2c). For Venus, this model suggests that the crust represents 0.8% of the silicate mass fraction of the planet, which is similar to Earth.

2.4.4. Mercury

Our knowledge of the thickness of Mercury's crust relies on non-unique gravity and topography inversions. Local crustal thickness inversions using GTR analysis and under the assumption of Airy isostasy provided an average crustal thickness of 35 ± 18 km (Padovan et al., 2015). Later improvements to the Airy isostasy formulation (Hemingway & Matsuyama, 2017 and see also Čadek et al., 2019) and crustal density estimates provided lower average crustal thicknesses of 26 ± 11 km together with relatively high crustal densities of $2,974 \pm 89$ kg m⁻³ (Sori, 2018). Global inversion of gravity data revealed the possibility of having a dynamic mantle support of longwavelength topography (James et al., 2015; Watters et al., 2021). A limitation to these models includes the fact that planetary crusts might strongly depart from isostatic equilibrium (as seen on the Moon and Mars; Neumann et al., 1996, 2004), such that this assumption might not be adequate when modeling the volcanically resurfaced crust of Mercury. Models considering a dynamic mantle also depend on an assumed interior viscosity structure, which is poorly known. Other crustal models investigated laterally and depth-variable crustal density (Beuthe et al., 2020) and considered crustal porosity (Broquet et al., 2024), though both assumed an average crustal thickness and density structure.

Our nominal model accounts for the effect of the laterally variable resolution of Mercury's gravity field, which is a major hindrance for the models (see Section 3 below), and assumes an average crustal thickness of 35 km and a constant crustal density of $2,800 \, \mathrm{kg \ m^{-3}}$, with a mantle density of $3,200 \, \mathrm{kg \ m^{-3}}$ (Figure 2d). In this model, crustal thickness ranges from 10 to 60 km and is lowest in regions covered by smooth plains, as is the case for the crust beneath the maria on the Moon. On Mercury, the crust is found to represent a substantial 9.3% of the silicate mass fraction of the planet, which is the highest value amongst the terrestrial planets.

BROOUET ET AL. 13 of 28

2.4.5. Earth

Compared to the terrestrial planets, lateral variations in the thickness of the Earth's crust are substantially more certain as a result of the extensive coverage of a global seismic network (Mooney et al., 2023). In the Earth's crust model of Mooney et al. (2023), the average crustal thickness is \sim 19 km. The crust further displays a bimodal distribution, being thicker in continents, \sim 40 km, with thickness exceeding 60 km in the Andes and Himalayas, and substantially thinner in the oceans, \sim 7 km (Figure S2 in Supporting Information S1).

3. Considerations to Improve Crustal Thickness Modeling

In this section, we present several considerations that can be used to improve a classical crustal thickness inversion. In particular, we describe approaches to account for the lateral variations in resolution of the planetary gravity field, avoid filtering the observed data and also consider a secondary layer with density variations in the crust and/or mantle. While some of these improvements are subject to non-uniqueness and do not result in a better fit to gravity and topography, we demonstrate that geologic arguments can be employed to favor some models over others. For additional discussion on depth and lateral variations in crustal density, we refer the reader to Goossens et al. (2020) (also Šprlák et al., 2020; Wahl et al., 2020) for the Moon and Beuthe et al. (2020) for Mercury. For further information on hydrostatic density interfaces in the mantle and core, see Wieczorek et al. (2019).

3.1. Accounting for Lateral Variations in Gravity Field Resolution

Compared to the topography of rocky bodies, which is generally well-resolved enough to probe the crust–mantle relief, the gravity field is poorly known (Table 2). Typically, the resolution of the gravity field at a given location is limited by the *degree-strength*, which represents the spherical harmonic degree at which the integrated acceleration uncertainty is above theoretical predictions (often based on the Kaula rule; Konopliv et al., 1999, 2020). Extreme cases of unevenly known gravity fields include Mercury, where global gravity field solutions are reliable up to only about spherical harmonic degree 10 (~1,500 km wavelength) in the southern hemisphere and extend to degree 90 and up to 160 in the north (~100–170 km; Konopliv et al., 2020). Although the BepiColombo mission will partially improve the gravity field in the southern hemisphere of the planet, post-BepiColombo gravity solutions are still expected to have important lateral variations in resolution (Iess et al., 2021). Venus also has an unevenly known gravity field, with resolution ranging from degree 40 to 100 (~940–380 km; Konopliv et al., 1999). Important lateral variations in resolution are anticipated to persist even after the EnVision and VERITAS missions, although the overall resolution is expected to improve to a range of 160–210 (Giuliani et al., 2025; Rosenblatt et al., 2021). The lateral variation in the resolution of the gravity field generally results from the elliptical orbit of radio-tracked spacecraft, such as Magellan for Venus or MESSENGER for Mercury (e.g., Genova et al., 2023).

To numerically resolve the issues related to an unevenly known gravity field, most previous studies either bandlimited their gravity and topography analyzes to a globally representative constant degree or strongly filtered short-wavelength gravity anomalies (e.g., Beuthe et al., 2020; James et al., 2015). However, this procedure biases geophysical inversions by exploiting wavelengths of topography smaller than those resolved in the gravity data in some regions while not allowing to utilize the gravity field at its full resolution elsewhere. An alternative approach to using global spherical harmonics is to construct shape models of the planet that account for the uneven resolution of the gravity field (Hikida & Wieczorek, 2007).

When working with spherical harmonics, one way to account for the variable resolution of the gravity field is to limit the spectral expansion of the Bouguer correction using a spatially variable maximum resolution before inverting for crustal thickness. For a function f with spatially variable spectral resolution L, the spectral degradation equation can be written as

$$f(\theta, \phi) = \sum_{l=0}^{L(\theta, \phi)} \sum_{m=-l}^{l} f_{lm} Y_{lm}(\theta, \phi)$$

In this equation, θ is the co-latitude, ϕ is the longitude, and l and m are the spherical harmonic degree and order, respectively (see also Mazarico et al., 2014). By spectrally limiting the expansion of the Bouguer correction to the

BROQUET ET AL. 14 of 28

000/2011/2012/2025JE009139 by Disch Zentrum F. Luft-U. Raum Fahrt In D. Helmholtz Gemei

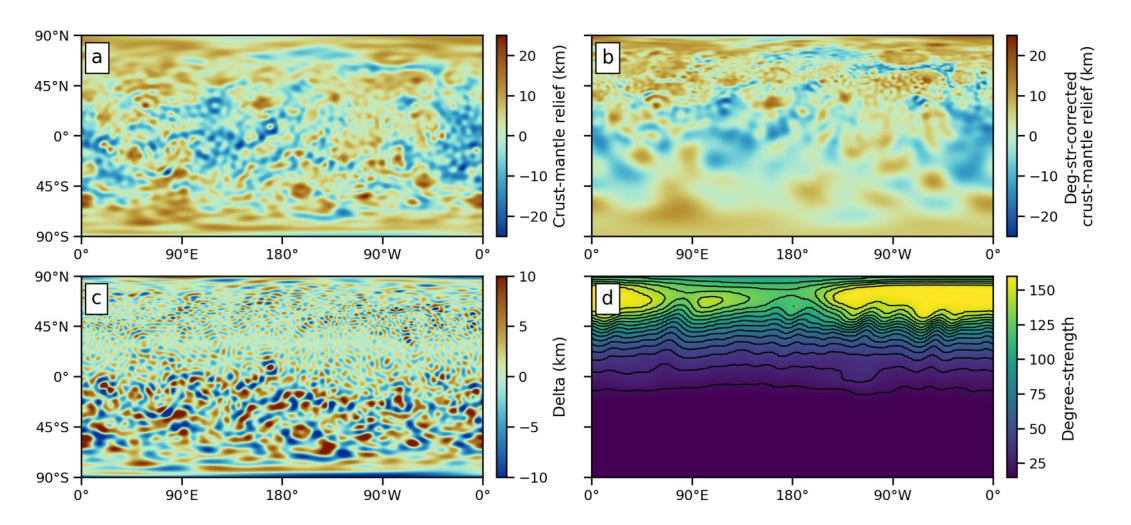


Figure 3. Effect of the degree-strength correction on the relief at the crust—mantle interface of Mercury. (a) Classical crust—mantle relief inversion and (b) our degree-strength corrected inversion. The difference between (a) and (b) is shown in (c). The degree-strength is shown in (d) with intervals of 10 degrees shown by black lines. The model in (a) shows an artificially exaggerated resolution that does not reflect our current knowledge of Mercury's gravity field.

laterally variable degree-strength, a crustal thickness inversion can fully leverage an unevenly known gravity field. This is achieved by using the above equation to compute a map of the Bouguer correction, re-expanding the map into spherical harmonics in order to obtain the degraded Bouguer correction coefficients. These coefficients are then subtracted from the free-air gravity anomaly to obtain the Bouguer anomaly that is then inverted for crustal thickness. One downside of this approach is that one cannot use a fast Fourier transform algorithm for computing global functions. However, as this approach is only needed once per input crustal density, it does not meaningfully slow down crustal thickness inversions.

To show the effect of this approach, we have inverted Mercury's crust—mantle relief using a classical approach and our degree-strength correction (Figure 3). In both cases, we use the gravity field and associated degree-strength models of Genova et al. (2023) (Table 2. Interestingly, we found the non-linear crust—mantle relief inversion to provide a stable solution for the degree-strength corrected model, whereas for the classic model the inversion did not converge. To stabilize the inversion, we added a low-pass damping filter with half-degree 90 (i.e., the spherical harmonic degree at which is filter equals 0.5) to the classical model, but also to the degree-strength corrected model for consistency. More information concerning the filtering process is provided in the next section.

For the classical model that does not consider the uneven resolution of Mercury's gravity field, the crust—mantle relief is seen to be well resolved in the southern hemisphere (Figure 3). However, this model is dominated by signals coming from the surface topography with little corresponding contribution from the smooth and low-resolution gravity field. This effect leads to a strong crustal thickness bias in the southern hemisphere that can lead to misinterpretation of the data. For example, small impact craters (<100 km) are more strongly expressed in the predicted crust—mantle relief of the southern hemisphere compared with the northern hemisphere. This is due to their numerically exaggerated effect on the Bouguer anomaly in regions with a low-resolution gravity field. When performing a degree-strength downsampling of the Bouguer correction, we obtain dramatic differences of more than ±15 km over a large fraction of the planet's southern hemisphere. In particular, we observe that impact craters are now absent from the southern hemisphere crust—mantle relief. Alternatively, to mitigate these effects, one could restrict the crustal thickness inversion to a low spherical harmonic degree as has been done in previous work (e.g., Beuthe et al., 2020). However, such an approach would prevent fully leveraging the higher-resolution gravity field in Mercury's northern hemisphere. In general, the degree-strength corrected model provides a more consistent representation of Mercury's crustal thickness given the current uncertainty in gravity data. This approach should be applied to planets for which the gravity field is strongly unevenly known, such as on Venus.

BROOUET ET AL. 15 of 28

3.2. Handling Short-Wavelength Gravity Anomalies

In a classical crustal thickness inversion, it is typically assumed that all Bouguer anomalies are due to relief at the crust-mantle interface. However, this assumption can cause the non-linear crustal thickness inversion to diverge. with the prediction of unrealistic short-wavelength oscillations of the crust-mantle interface (amplitudes of ±100 km and more). These oscillations result from the often-incorrect assumption that short-wavelength Bouguer gravity anomalies (degree >80) are due to variations in crustal thickness rather than density. On the Moon, analyzes of GRAIL data have shown that the dominant high-degree Bouguer gravity signal is in the form of pervasive small-scale gravity anomalies, with size and magnitude comparable to many discrete structures, including linear intrusions or ring dikes around basins (Broquet & Andrews-Hanna, 2024b; Jansen et al., 2017). The small-scale Bouguer gravity anomalies were further found to be consistent with crustal density variations of ±150 kg m⁻³ embedded within the top 20 km of the crust (Jansen et al., 2017). In addition, one expects shortwavelength and steep relief variations of the crust-mantle interface to either relax on geologic timescales due to the warmer temperature and high lateral pressure gradient at these depths (Nimmo & Stevenson, 2001) or be eroded by advective flows in the mantle (Davies, 1994). On the Moon, viscoelastic modeling by Mohit and Phillips (2006) indicates that under relatively high heat flows of 35 mW m⁻², tens of kilometer of Moho relief at ~200 km wavelength (equivalent to degree 55) fully relaxes in only about 500 Myr (see also Zhu et al., 2025). Even faster relaxation times would be expected for shorter wavelengths and warmer planets, such as Venus or Mars (Mohit & Phillips, 2007). Together, these considerations suggest that short-wavelength Bouguer gravity anomalies should generally not be directly related to variations in the relief of the crust-mantle interface.

To avoid these issues, a low-pass filter is typically applied to damp the effect of short-wavelength Bouguer anomalies on the crustal thickness inversion. Previous studies have designed filters based on a formulation that minimize the amplitude or curvature of the crust-mantle interface in Cartesian space (Parker, 1973; Phipps Morgan & Blackman, 1993) and on a sphere (Wieczorek & Phillips, 1998) or based on simpler cosine functions (Andrews-Hanna et al., 2018). The main difference is the attenuation of long-wavelength gravity anomalies, which can be up to a few percent for the minimum-amplitude or -curvature filters. The half-degree, or spherical harmonic degree at which the filter is equal to 0.5, is generally chosen such that the crustal thickness inversion does not diverge or display unrealistic oscillations at high spherical harmonic degrees. On the Moon, filters with half-degree 80 were considered (Wieczorek et al., 2013) compared to 50 for Mars (Wieczorek et al., 2022) or 40 for Mercury (Beuthe et al., 2020). Importantly, the filter also mitigates uncertainties in gravity data (where the inversion resolution exceeds the degree-strength), which are more pronounced at short-wavelengths and are exponentially amplified by the downward continuation of the Bouguer anomaly to the crust-mantle interface. While this effect may be important for Mars or Mercury, the small uncertainties in GRAIL gravity data on the Moon do not affect crustal thickness inversions. Thus, for the Moon, the divergence (or non-convergence) of the crustal thickness inversion when using short-wavelength gravity data is unrelated to noise and is rather due to incorrect modeling assumptions.

One critical issue with such a filtering approach is that a non-negligible fraction of the gravity field is discarded. An alternative is to simultaneously solve for lateral variations in crustal density and thickness. Assumptions on how crustal density varies with depth can be supplied (i.e., near surface or density decrease with depth), but for simplicity, we here assume crustal density to be constant with depth, from the surface to the base of the crust. Rather than filtering out and excluding short-wavelength gravity anomalies, these are ascribed to crustal density and feedback into the estimation of the crustal thickness. Similar to a crustal inversion model, this approach is iterative. A first crustal thickness model is made with short-wavelength Bouguer gravity anomalies being partially excluded, as would be the case in a classical filtered inversion. These short-wavelength anomalies are saved and in a new model, they are inverted for crustal density variations in a constant thickness shell. A new crustal thickness model is made using the derived density variations and this process is repeated until convergence. Combined with our degree-strength downsampling approach, this additional step enables a crustal thickness model to fully leverage available data and provide a self-consistent model of crustal thickness and density.

To show the effect of this approach, we have inverted Mars' crustal structure using a classical approach and our combined crustal density and thickness inversion (Figure 4). A half-degree 50 filter is used to discard short-wavelength Bouguer anomalies in the classical model (see Figure 4a), as has been used in previous work to make the inversion converge and not display unrealistic oscillations (Wieczorek et al., 2022). In our updated model, the discarded data is used to invert for crustal density and the rest is used to estimate crustal thickness

BROOUET ET AL. 16 of 28

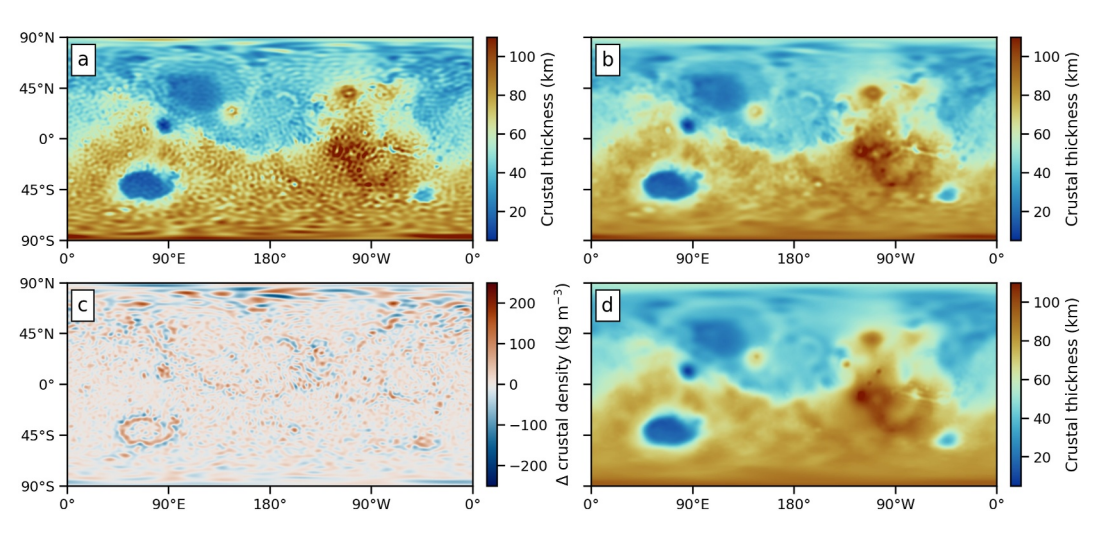


Figure 4. Effect of low-pass filtering on a Martian crustal thickness inversion. Crustal thickness model with no filtering displaying unrealistic crustal thickness oscillations (a) and when using a low-pass filter with half-degree 50 (b). Crustal density variation with respect to a mean of 2,900 kg m $^{-3}$ (c) and associated crustal thickness (d) both for a self-consistent unfiltered model that ascribes short-wavelength anomalies to density variations in the crust.

following the above iterative approach. Our global inversion is performed up to degree 90, which is the global average degree-strength of Mars' gravity field. As for other planets, Mars gravity field models have uneven degree-strengths, reaching degree ~80 in the northern hemisphere versus ~100 in the south. This implies that some of our inferred short-wavelength crustal density anomalies in the northern hemisphere could be slightly affected by noise in the gravity data.

A notable effect is that our approach leads to a smoother crustal thickness map that fully fits the observed gravity and that better represents the geology of the planet. The classical model crustal coarseness is due to the filter discarding a portion of the data, leading to sharp crustal thickness variations whose wavelength depends on the shape of the low-pass filter (compare Figures 4b and 4d). As this model matches the observed gravity only with crustal thickness variations, this gives rise to more power at short wavelengths. When considering the gravity contribution from crustal density variations, our updated model predicts more realistic crustal thickening at smallscale features such as Tharsis volcanoes, with crustal densities (~3,000–3,100 kg m⁻³) consistent with earlier work (Figure S3 in Supporting Information S1; Broquet & Wieczorek, 2019). Seemingly random and pervasive density anomalies of $\pm 200 \text{ kg m}^{-3}$ are obtained, which is reminiscent of previous work mapping intrusions and porosity variations on the Moon (Jansen et al., 2017). Relatively small impact craters (<300 km) are also generally less visible, which is more consistent with them not puncturing the crust but affecting the upper crust density from impact-induced brecciation and with the formation of low-density ejecta blankets. We note that Bouguer anomalies interpreted as density variations in our model are observed in the vicinity of large impact basins, such as Hellas and Argyre, or across the dichotomy boundary. These anomalies are more likely to be associated with sharp crustal thickness variations (rather than density as defined here) as they closely follow crustal discontinuities. Using a filter with a larger half-degree would help resolve this issue but would also affect other regions.

We note that this improved approach still requires an external assumption regarding how gravity is partitioned in terms of crustal thickness and density (here with our half-degree 50 filter) as well as where density anomalies are located. For example, if the short-wavelength anomalies were attributed to density variations in the upper crust (rather than the whole crust), the inverted density variations would generally have larger magnitudes. In addition, and as further discussed in the section below, long-wavelength variations in crustal density are also expected on Mars and in particular in the thick basaltic crust of the Tharsis plateau. Thus, although our suggestion to better handle short-wavelengths improves crustal thickness models by allowing them to exploit more data and be self-consistent, our model still depends upon an assumption concerning the wavelength and depth dependence of crustal density. The reliability of the model will thus depend upon how closely accurate the employed assumption is. Nevertheless, our approach should generally be preferred over inversions that discard observations.

BROOUET ET AL. 17 of 28

com/doi/10.1029/2025IE009139 by Dtsch Zentrum F. Luft-U. Raum Fahrt In D. Helmholtz Gemei

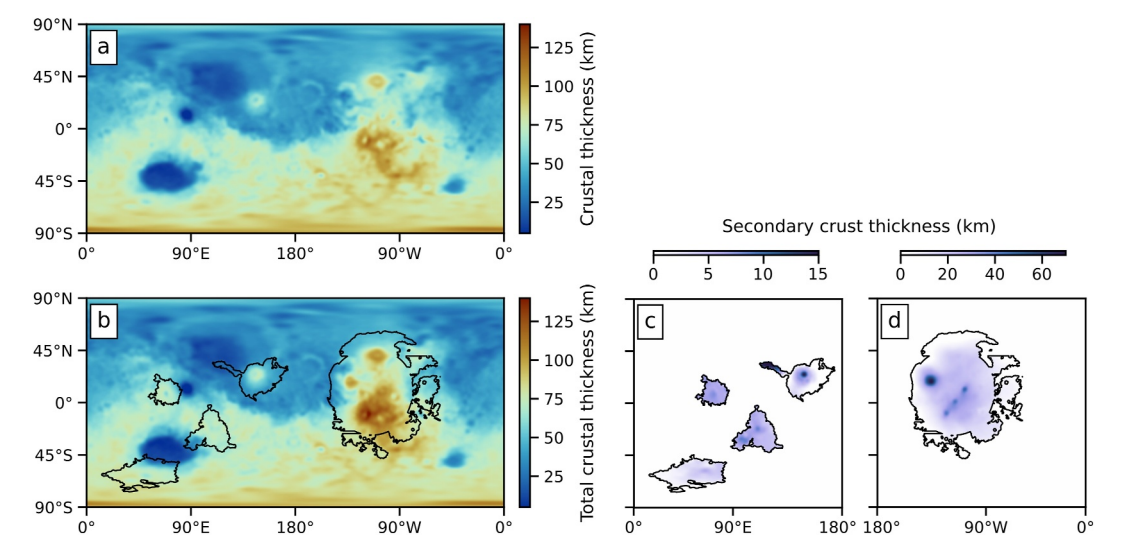


Figure 5. Effect of considering a higher-density secondary crust on a Martian crustal thickness inversion. (a) Classical single-layer crustal thickness inversion. (b) Total crustal thickness considering a two-layer inversion under the premise of prevolcanism crustal isostasy in the Tharsis, Elysium, and Hesperian volcanic provinces. The thickness of the secondary crust considering two color-scales on the western (c) and eastern (d) hemispheres.

3.3. A Non-Isostatic Secondary Crust: The Case of Mars

Due to a lack of observational constraints on the lateral variation of interior properties, classical crustal inversions typically consider a constant density mantle and crust. Some notable studies have considered lateral and depth variations in the bulk density of the crust, as inferred from high-resolution gravity data (Besserer et al., 2014; Goossens et al., 2017; Šprlák et al., 2020; Wahl et al., 2020; Wieczorek et al., 2013), and/or spectrometers in orbit (Baratoux et al., 2014; Beuthe et al., 2020), but also from porosity estimates (Broquet et al., 2024).

While lateral and depth variations in crustal and mantle density are expected for all terrestrial bodies, some planets such as Mars or the Moon host a voluminous secondary crust that is substantially denser than the surrounding crust. This intra-crustal layering induces a gravitational anomaly that when considered can affect crustal thickness estimates, such as for the mare-covered basins on the Moon (Broquet & Andrews-Hanna, 2024a; Wieczorek & Phillips, 1999). However, adding a supplementary layer with unknown relief (i.e., not parallel to topography) makes a crustal thickness inversion under-determined. In the case of an early-formed crust, one can plausibly assume that the crust should have initially been in isostatic equilibrium and that this state would have been frozen into the lithosphere as the planet cooled. However, a secondary crust forming later on a cooling planet is expected to depart from isostasy. As the secondary crust forms, it would bend the underlying isostatically frozen crust and lithosphere and create a strong non-isostatic gravity anomaly. On the Moon, the work of Broquet and Andrews-Hanna (2024a) used the assumption of long-wavelength isostasy to simultaneously infer the relief between the secondary basaltic crust (i.e., mare) and feldspathic crust and between the feldspathic crust and the underneath mantle. Mars is also thought to have gone through a magma ocean phase during which the bulk of the crust quickly crystallized, which makes the assumption of long-wavelength isostasy appropriate (Bouvier et al., 2018). Previous work by Ritzer and Hauck (2009) has also assumed isostasy to describe the Isidis basin's post-impact crustal structure and to estimate the thickness of lava flows and flexural deformation.

Here, we build upon the framework developed by Broquet and Andrews-Hanna (2024a) to create a two-layer crustal thickness model for Mars. This model assumes that a 3,100 kg m⁻³ secondary crust overlies a prevolcanism isostatic lower-density crust (2,800 kg m⁻³) in the Tharsis, Elysium and Hesperian volcanic provinces, as mapped by Tanaka et al. (2014) (Figure 5). For simplicity, this model doesn't account for other volcanic units which likely have thicknesses of only several hundreds of meters to a few kilometers, such as in Elysium Planitia (e.g., Voigt et al., 2023) or in the northern lowlands (Head et al., 2002). Due to its higher density, the secondary basaltic crust acts as a load that will bend all crustal interfaces, depending on the rigidity of the planet's interior. In our DSP model, thin elastic shell theory is used to predict this bending as a function of the lithosphere elastic thickness (Broquet, 2024a; Broquet & Andrews-Hanna, 2023a). The elastic thickness of the lithosphere is

BROQUET ET AL. 18 of 28



assumed to be 80 km, which is required to support the large-scale Tharsis load (Andrews-Hanna et al., 2008). We note that most shield volcanoes on Mars formed on a thinner elastic lithosphere of <15 km (Broquet & Wieczorek, 2019), but the lithosphere there was likely eroded by small-scale mantle plumes, as is the case in Hawaii (e.g., Davies, 1994). Larger elastic thicknesses are also found beneath the Martian polar caps, >150 km, but these formed and deformed the lithosphere later in geologic history when the planet was colder (e.g., Broquet et al., 2020). Under these assumptions, the thickness of the secondary, basaltic crust is found to be \sim 30 km in the Tharsis province and to range from 70 km at Olympus Mons (\sim 50% of the total regional crust thickness) to 15 km for Elysium Mons and <7 km for smaller-scale volcanoes in Hesperian volcanic provinces, such as Tyrrhena Mons. The volume of the secondary crust is constrained to be \sim 3 × 10⁸ km³, consistent with earlier work (Phillips et al., 2001). We note that the aforementioned values strongly depend on the thickness of the elastic lithosphere, which has varied in space and time from a few kilometers to tens of kilometers (e.g., Broquet & Wieczorek, 2019). A full investigation of the influence of these effects on Mars' crustal structure is out of the scope of this study.

When considering a secondary basaltic crust, the total thickness of the crust is increased by 5–50 km in volcanic provinces (Figure 5). The thickest crust is now found at Arsia Mons with values reaching 135 km for the model with the secondary crust, 25 km thicker than when not accounting for it. Volcanic constructs such as Olympus Mons or Alba Mons are also seen to have a more pronounced localized crustal thickening compared to the surrounding crust. This is due to a part of the gravitation signal of these regions being compensated at the secondary–primary crust interface with a density contrast of 200 kg m $^{-3}$ that is smaller than that at the crust–mantle interface (\sim 500 kg m $^{-3}$). Thus, considering the higher density of the crust in volcanic provinces will thicken the crust in these regions and match the expectation of a volcanically thickened crust near individual large volcanoes.

3.4. Mantle Density Anomalies: The Case of Venus and the Moon

Venus and Mercury have shown evidence for long-wavelength support of their topography by density anomalies in the mantle resulting from interior dynamics (James et al., 2013, 2015) or surface temperature effects (Tosi et al., 2015). Planetary mantles are also expected to display important density variations, resulting from non-even cooling below crusts enriched in heat-producing elements and of variable thickness (Breuer & Moore, 2015). All these effects would generate gravitational anomalies that would affect the estimation of crustal thickness from gravity data. As noted above and because of the depth-attenuation of gravity anomalies, considering mass anomalies in the mantle will mostly affect the long-wavelength structure of the crust. Mantle mass anomalies will also tradeoff with crustal thickness. For example, a positive gravity anomaly could be either interpreted as a flat crust with mass excess in the mantle or as a thinned crust with a constant-density mantle.

Here, we invert Venusian gravity and topography for global crustal thickness. For the longest wavelengths, we consider the contribution of a dynamic mantle load located within a 400 km thick shell that sits directly below an isostatic crust. At shorter wavelengths, we assume crustal compensation and the isostasy assumption is relaxed. The transition between the long-wavelength hybrid support and crustal compensation only is modeled using a cosine taper with half-degree 15. This spherical harmonic degree corresponds to the wavelength at which the topography of Venus is thought to transition from being supported dynamically in the mantle to more passively by crustal thickening (James et al., 2013). Given the tradeoff between the mantle load thickness and density, choosing a thinner mantle load would lead to larger-magnitude density variations with minimal effects on crustal thickness. This consideration leads to the near-disappearance of a crustal thickening at Atla Regio and Beta Regio and to an overall decrease in crustal thickness at crustal plateaus, when compared to a classical model (Figure 6). For example, crustal thickness at Ovda Regio decreases from 37 to 33 km and from 60 to 50 km at Ishtar Terra when considering our mantle contribution to the gravity field. These regions are further seen to overlie major mantle upwellings, as indicated by negative mantle density contrasts, which is consistent with earlier work (e.g., James et al., 2013; Maia et al., 2023; Pauer et al., 2006). Interestingly, regions with predicted mantle upwelling correlate with the location of 80% of potentially active Coronae mapped in Gülcher et al. (2020). This suggests that long-wavelength mantle upwellings, which interact and potentially trigger Venus' volcano-tectonic activity, can be resolved in observed gravity and topography data. In our model, mantle density anomalies are found to range from -30 to 30 kg m⁻³ about a mean of 3,300 kg m⁻³, implying temperature contrasts of ± 300 K for a thermal expansivity of $3 \times 10^{-5} \text{ K}^{-1}$. Such temperature variations are consistent with the expected spatial variability in Venusian heat flow (S. E. Smrekar et al., 2023). Note that for crustal thickness, our model is unable to constrain absolute mantle densities. For Mercury, a similar approach has a substantial effect on crustal

BROOUET ET AL. 19 of 28

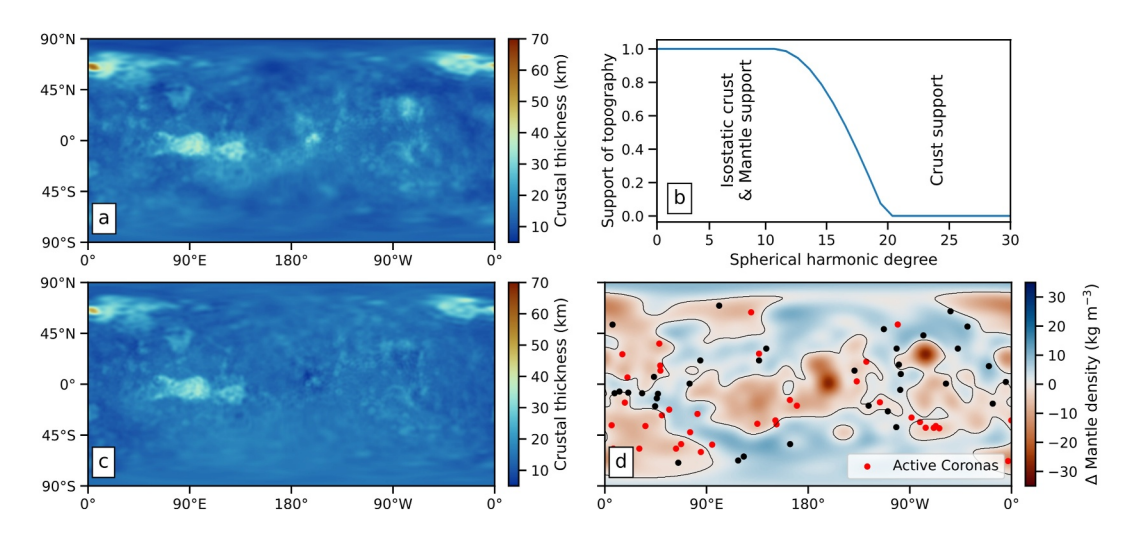


Figure 6. Effect of considering a long-wavelength dynamic mantle and isostatic crust on Venusian crustal thickness. (a) Crustal thickness inversion with crustal support only. (b) Transition filter for the mantle/crust support model, with the associated crustal thickness (c) and mantle density variations (d). Coronae mapped by Gülcher et al. (2020) are indicated by the dots in (d), with the active ones shown in red. Negative mantle density contrasts indicate regions with hot mantle upwellings.

thickness estimates and provides mantle density variations reflecting the planet's surface temperature pattern (Figure S4 in Supporting Information S1), which is thought to extend deep down in the mantle (Fleury et al., 2024; Tosi et al., 2015).

Lunar thermal evolution models predict important interior temperature anomalies resulting from the high heat production of the Procellarum KREEP Terrane (Laneuville et al., 2018; Wieczorek & Phillips, 2000). These models predict the present-day nearside mantle to be hotter than the farside mantle, which is consistent with recent analyzes of time-variable gravity data from GRAIL (Park et al., 2025). In the models of Laneuville et al. (2013), the difference in temperature between the warmer nearside Procellarum region and farside can reach several hundred Kelvin from the surface down to the mid-mantle. In Figure 7, we illustrate the effect on crustal thickness of a present-day 400 K mantle temperature anomaly located beneath the Procellarum region, ranging from the base of the crust to 200 km depth. Importantly, we note that this example neglects the effect of possible compositional differences on mantle density that could arise from the extraction of mare basalts or the presence of

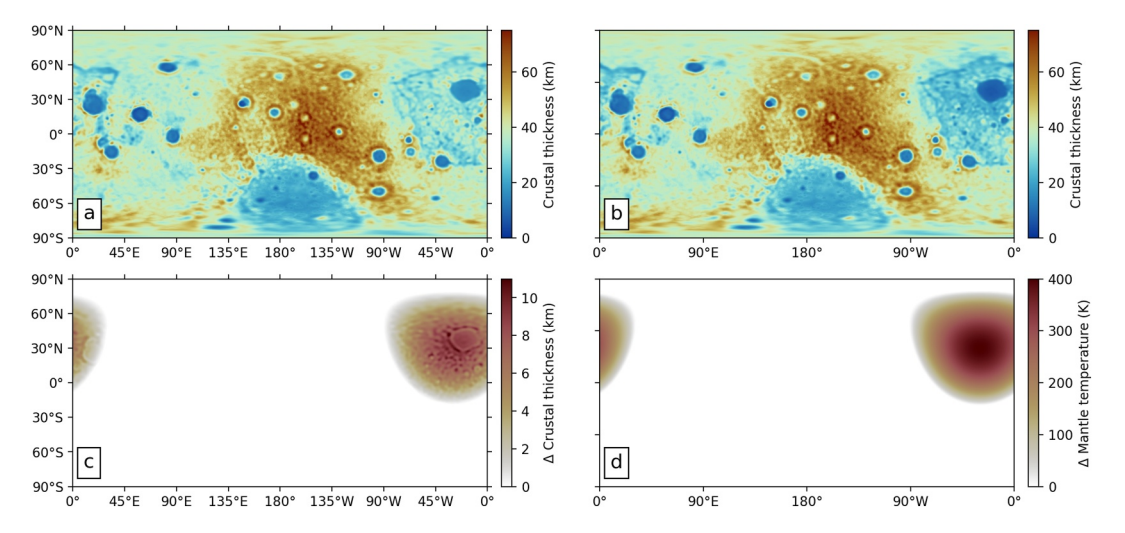


Figure 7. Effect of considering a 400 K warmer mantle in the Procellarum region on a crustal thickness inversion. (a) Classical crustal thickness inversion. Hybrid model considering crustal thickness (b) and mantle density variations (d). The difference between (a) and (b) is shown in (c).

BROQUET ET AL. 20 of 28



ilmenite-rich magma ocean cumulates. Additional considerations on the effect of temperature, compositional anomalies, and intrusions on the gravity field can be found in Laneuville et al. (2013). Here, gravity and topography are inverted for crustal thickness considering the contribution from the mantle density anomaly directly beneath the Procellarum region. When compared to a model neglecting this thermal anomaly, accounting for a warmer nearside mantle leads to a crustal thickness reduction of about 10 km beneath the Procellarum region (~30% of the regional crust thickness). This effect further reinforces the global asymmetry in the lunar crust. Crustal thickness estimates at the Apollo 12 and 14 landing sites are also predicted to be 3–4 km thinner. Together, these would affect how local seismic measurements of crustal thickness are related to the global properties of the Moon.

4. Discussion and Conclusions

The thickness of a planet's crust varies in space and time, and exerts a prominent control on the geologic and geodynamic evolution of the interior. In this work, we have provided a broad overview of our current knowledge of the composition and structure of planetary crusts. The Moon and Mars display thick crusts with substantial lateral variations. The crustal architecture of these bodies is relatively well known, as a result of seismic stations on their surface and due to our relatively good knowledge of their gravity fields. The crust of Mercury and Venus is substantially less known, but both planets might have thinner and denser crusts with less pronounced variability. Future space missions to these two bodies will allow for major improvements in our understanding of their crustal structure. In general, planetary crusts represent less than a percent (Venus, Earth) and up to several percent of the silicate mass fraction of the planet (Mercury, Mars, the Moon).

Considerations to improve gravity and topography inversion models for crustal thickness have been proposed. Accounting for the effect of an unevenly known gravity field or variations in crustal and mantle densities were shown to lead to dramatic variations in our crustal thickness models. For Mercury, degree-strength downsampling of the Bouguer anomaly is necessary to avoid misinterpreting the crustal thickness inversions. While crustal thickness models remain non-unique and subject to assumptions regarding the origin of gravity anomalies, we have demonstrated that some solutions can be favored based on geologic arguments. For example, ascribing short-wavelength gravity anomalies to crustal density on Mars was found to provide a more geologically realistic structure for the crust beneath the large volcanic constructs. On the Moon, the location of grabens near mare basins can be used to provide constraints on the structure of the crust, including mare thickness (Broquet & Andrews-Hanna, 2024a; Solomon & Head, 1980). A similar approach could be undertaken to refine estimates on the thickness of Mars' secondary basaltic crust based on circum-Tharsis tectonics and in other volcanically flooded regions (see also Andrews-Hanna & Broquet, 2023). Accounting for a non-isostatic long-wavelength mantle on Venus leads to the prediction of mantle upwellings in regions with potentially active Coronae (see also James et al., 2013). As discussed for Mars and the Moon, the Venusian tectonic record could also be used to further constrain the interior structure. A similar approach on Mercury provided long-wavelength mantle temperatures that reflect the present-day surface temperature pattern (see also Tosi et al., 2015). Finally, we have shown that forward modeling of expected temperature contrasts in the lunar mantle leads to non-negligible crustal thickness differences between the near and far sides, with implications for how seismically constrained crustal thicknesses at the Apollo landing sites are related to global lunar properties. If successful, the future Farside Seismic Suite will provide major constraints on the thickness of the farside crust (Panning et al., 2024), thereby reducing the range of possible crustal thickness models.

Lateral and depth variations in the bulk density of the crust are the primary factors affecting crustal thickness estimation. While the surface composition of planetary bodies is generally well known, it remains unclear whether the density of surface materials is representative of the bulk crust. Crustal porosity, which prominently affects bulk density, is also expected to vary substantially and continue to be challenging to constrain. The collection of high-resolution gravity data may allow inferring the bulk density of the upper crust using localized admittance techniques. For the Moon, high-resolution GRAIL data allowed constraining a low bulk density of the crust of ~2,550 kg m⁻³ (Wieczorek et al., 2013). For Mars, this approach provided a low globally average bulk density of ~2,600 kg m⁻³ (Goossens et al., 2017), though with values as high as 3,200 kg m⁻³ at Martian volcanoes (Broquet & Wieczorek, 2019; Goossens et al., 2017). However, Mars' lower resolution gravity field causes crustal density estimates to tradeoff with over parameters including the elastic thickness of the lithosphere. As shown in Figure 8, a resolution of at least spherical harmonic degree 200 (wavelength of ~100 km) globally

BROOUET ET AL. 21 of 28

com/doi/10.1029/2025JE009139 by Disch Zentrum F. Luft-U. Raum Fahrt In D. Helmholtz Gemein., Wiley Online Library on [07/10/2025]. See the Term

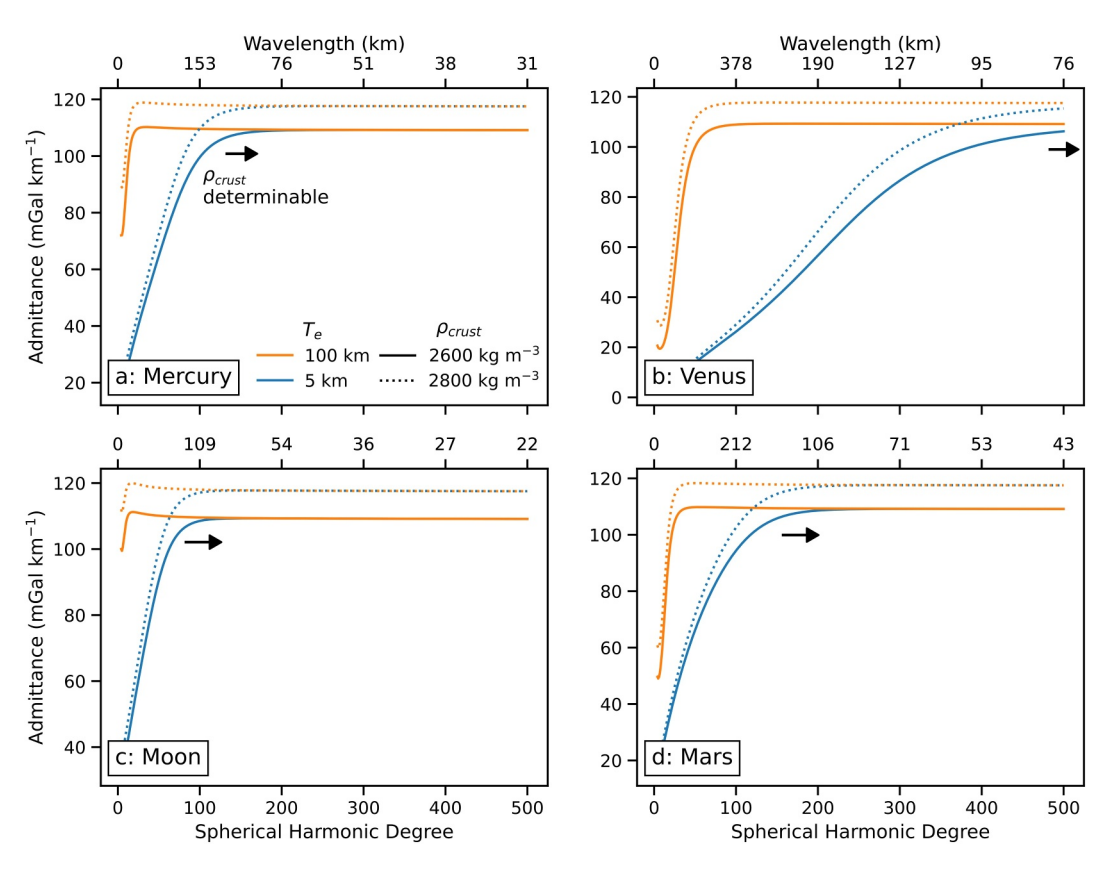


Figure 8. Sensitivity of global admittance models as a function of spherical harmonic degree, elastic thickness (T_e) and crustal density (ρ_{crust}) for Mercury (a), Venus (b), the Moon (c) and Mars (d). The arrow indicates the spherical harmonic degree range at which crustal density can be determined independently from elastic thickness. Admittances were computed using the Py_Admittance package (Broquet, 2024b).

would allow to disentangle these parameters. On Venus, due to the planet's larger size and smaller membrane stresses, crustal density can be independently constrained only for a higher spherical harmonic degree of >500 (wavelength <80 km). However, we note localized admittance studies might be able to fully decouple crustal density and thickness at Veritas and EnVision gravity resolutions. For the smaller Mercury, crustal density can be unambiguously determined for spherical harmonic degrees greater than about 180 (wavelength of 85 km). Nevertheless, we emphasize that admittance analyzes may be sensitive only to the upper few kilometers of the surface, which could complicate the interpretation of the admittance function. As a result, the inferred crustal density may not accurately reflect the density contrast at the crust–mantle boundary that has a prominent effect on a crustal thickness inversion.

Our relatively poor knowledge of planetary gravity fields remains the main frontier to bridge in order to improve our understanding of the crustal architecture of planetary crust. Dedicated gravity recovery missions to the terrestrial planets (Genova, 2020; Giuliani et al., 2025; Iess et al., 2021; Rosenblatt et al., 2021; Wörner et al., 2023) will allow to perfect our gravity and crustal thickness models as well as unveil much of the tectonic, magmatic, and geodynamic history of these worlds.

Data Availability Statement

Inversions presented in this manuscript have used DSP (Broquet, 2024a), Py_Admittance (Broquet, 2024b), ctplanet (Wieczorek, 2024) and SHTOOLs (Wieczorek et al., 2024). Gravity and topography data can be found at the pds-geosciences node (https://pds-geosciences.wustl.edu/) and some colormaps are from Crameri (2018). The nominal crustal thickness models presented in Figure 2 are available at Broquet (2025).

BROQUET ET AL. 22 of 28

Acknowledgments

A.B. is supported by the Alexander von Humboldt Foundation. The authors thank Associate Editor Mike Sori, Reviewer Peter James, and an anonymous reviewer for their detailed comments, which helped improve the manuscript. Open Access funding enabled and organized by Projekt DEAL.

References

- Anderson, F. S., & Smrekar, S. E. (2006). Global mapping of crustal and lithospheric thickness on Venus. *Journal of Geophysical Research*, 111(E8). https://doi.org/10.1029/2004je002395
- Andrews-Hanna, J. C., & Broquet, A. (2023). The history of global strain and geodynamics on Mars. *Icarus*, 395, 115476. https://doi.org/10.1016/j.icarus.2023.115476
- Andrews-Hanna, J. C., Head, J. W., Johnson, B. C., Keane, J. T., Kiefer, W. S., McGovern, P. J., et al. (2018). Ring faults and ring dikes around the Orientale basin on the Moon. *Icarus*, 310, 1–20. https://doi.org/10.1016/j.icarus.2017.12.012
- Andrews-Hanna, J. C., Zuber, M. T., & Hauck, S. A. I. I. (2008). Strike-slip faults on Mars: Observations and implications for global tectonics and geodynamics. *Journal of Geophysical Research*, 113, E08002. https://doi.org/10.1029/2007JE002980
- Armann, M., & Tackley, P. J. (2012). Simulating the thermochemical magmatic and tectonic evolution of Venus's mantle and lithosphere: Two-dimensional models. *Journal of Geophysical Research*, 117(E12), E12003. https://doi.org/10.1029/2012JE004231
- Banerdt, W. B. (1986). Support of long-wavelength loads on Venus and implications for internal structure. *Journal of Geophysical Research*, 91(B1), 403–419. https://doi.org/10.1029/JB091iB01p00403
- Banerdt, W. B., Smrekar, S. E., Banfield, D., Giardini, D., Golombek, M., Johnson, C. L., et al. (2020). Initial results from the InSight mission on Mars. *Nature Geoscience*, 13(3), 183–189. https://doi.org/10.1038/s41561-020-0544-y
- Baratoux, D., Samuel, H., Michaut, C., Toplis, M. J., Monnereau, M., Wieczorek, M., et al. (2014). Petrological constraints on the density of the
- Martian crust. Journal of Geophysical Research: Planets, 119(7), 1707–1727. https://doi.org/10.1002/2014JE004642
 Becker, K. J., Robinson, M. S., Becker, T. L., Weller, L. A., Edmundson, K. L., Neumann, G. A., et al. (2016). First global digital elevation model
- of Mercury. In 47th Lunar & Planetary Science Conference (Vol. 2959).
 Benkhoff, J., Murakami, G., Baumjohann, Besse, S., Bunce, E., Casale, M., et al. (2021). BepiColombo—Mission overview and science goals.
- Space Science Reviews, 217(8), 90. https://doi.org/10.1007/s11214-021-00861-4
- Besserer, J., Nimmo, F., Wieczorek, M. A., Weber, R. C., Kiefer, W. S., McGovern, P. J., et al. (2014). GRAIL gravity constraints on the vertical and lateral density structure of the lunar crust. *Geophysical Research Letters*, 41(16), 5771–5777. https://doi.org/10.1002/2014GL060240
- Beuthe, M., Charlier, B., Namur, O., Rivoldini, A., & Van Hoolst, T. (2020). Mercury's crustal thickness correlates with lateral variations in mantle melt production. *Geophysical Research Letters*, 47(9), e2020GL087261. https://doi.org/10.1029/2020GL087261
- Bills, B. G., & Ferrari, A. J. (1977). A lunar density model consistent with topographic, gravitational, librational, and seismic data. *Journal of Geophysical Research*, 82(8), 1306–1314. https://doi.org/10.1029/JB082i008p01306
- Bonnet Gibet, V., Michaut, C., Bodin, T., Wieczorek, M., & Dubuffet, F. (2025). Martian highlands differentiation concomitant to dichotomy formation. *Journal of Geophysical Research: Planets*, 130(3), e2024JE008486. https://doi.org/10.1029/2024JE008486
- Bouvier, L. C., Costa, M. M., Connelly, J. N., Jensen, N. K., Wielandt, D., Storey, M., et al. (2018). Evidence for extremely rapid magma ocean crystallization and crust formation on Mars. *Nature*, 558(7711), 586–589. https://doi.org/10.1038/s41586-018-0222-z
- Breuer, D., & Moore, W. B. (2015). Dynamics and thermal history of the terrestrial planets, the Moon, and Io. In *Treatise on geophysics* (2nd ed., Vol. 10, pp. 255–305). https://doi.org/10.1016/B978-0-444-53802-4.00173-1
- Broquet, A. (2024a). AB-Ares/Displacement_strain_planet: Version 0.5.0. Zenodo. https://doi.org/10.5281/zenodo.10552129
- Broquet, A. (2024b). AB-Ares/Py_Admittance: Version 0.1.0. Zenodo. https://doi.org/10.5281/zenodo.10925820
- Broquet, A. (2025). Data for on the crustal architecture of the terrestrial planets [Dataset]. Zenodo. https://doi.org/10.5281/zenodo.15181140
- Broquet, A., & Andrews-Hanna, J. C. (2023a). Geophysical evidence for an active mantle plume underneath Elysium Planitia on Mars. *Nature Astronomy*, 7. https://doi.org/10.1038/s41550-022-01836-3
- Broquet, A., & Andrews-Hanna, J. C. (2023b). Plume-induced flood basalts on Hesperian Mars: An investigation of Hesperia Planum. *Icarus*, 391, 115338, https://doi.org/10.1016/j.icarus.2022.115338
- Broquet, A., & Andrews-Hanna, J. C. (2024a). The Moon before mare. *Icarus*, 408, 115846. https://doi.org/10.1016/j.icarus.2023.115846
 Broquet, A., & Andrews-Hanna, J. C. (2024b). A volcanic inventory of the Moon. *Icarus*, 411, 115954. https://doi.org/10.1016/j.icarus.2024.
- Broquet, A., Plesa, A. C., Klemann, V., Root, B. C., Genova, A., Wieczorek, M. A., et al. (2025). Glacial isostatic adjustment reveals Mars's interior viscosity structure. *Nature*, 639(8053), 109–113. https://doi.org/10.1038/s41586-024-08565-9
- Broquet, A., Rolser, F., Plesa, A. C., Breuer, D., & Hussmann, H. (2024). Mercury's crustal porosity as constrained by the planet's bombardment history. *Geophysical Research Letters*, 51(21), e2024GL110583, https://doi.org/10.1029/2024GL110583
- Broquet, A., & Wieczorek, M. A. (2019). The gravitational signature of Martian volcanoes. *Journal of Geophysical Research: Planets*, 124(8), 2054–2086. https://doi.org/10.1029/2019JE005959
- Broquet, A., Wieczorek, M. A., & Fa, W. (2020). Flexure of the lithosphere beneath the north polar cap of Mars: Implications for ice composition and heat flow. *Geophysical Research Letters*, 47(5), e2019GL086746. https://doi.org/10.1029/2019GL086746
- Broquet, A., Wieczorek, M. A., & Fa, W. (2021). The composition of the south polar cap of Mars derived from orbital data. *Journal of Geophysical Research: Planets*, 126(8), e2020JE006730. https://doi.org/10.1029/2020JE006730
- Byrne, P. K. (2020). A comparison of inner Solar System volcanism. *Nature Astronomy*, 4, 321–327. https://doi.org/10.1038/s41550-019-0944-3 Čadek, O., Souček, O., & Běhounková, M. (2019). Is Airy isostasy applicable to icy moons? *Geophysical Research Letters*, 46(24), 14299–14306. https://doi.org/10.1029/2019GL085903
- Campbell, B. A., Morgan, G. A., Whitten, J. L., Carter, L. M., Glaze, L. S., & Campbell, D. B. (2017). Pyroclastic flow deposits on Venus as indicators of renewed magmatic activity. *Journal of Geophysical Research: Planets*, 122(7), 1580–1596. https://doi.org/10.1002/2017JE005299
- Carr, M. H., & Head, J. W. (2010). Geologic history of Mars. Earth and Planetary Science Letters, 294(3–4), 185–203. https://doi.org/10.1016/j.epsl.2009.06.042
- Chenet, H., Lognonné, P., Wieczorek, M. A., & Mizutani, H. (2006). Lateral variations of lunar crustal thickness from the Apollo seismic data set. Earth and Planetary Science Letters, 243, 1. https://doi.org/10.1016/j.epsl.2005.12.017
- Crameri, F. (2018). Scientific colour maps: Perceptually uniform and colour-vision deficiency friendly. Zenodo. https://doi.org/10.5281/zenodo. 1243862
- Davies, G. F. (1994). Thermomechanical erosion of the lithosphere by mantle plumes. *Journal of Geophysical Research*, 99(B8), 15709–15722. https://doi.org/10.1029/94JB00119
- Durán, C., Khan, A., Ceylan, S., Zenhäusern, G., Stähler, S., Clinton, J., & Giardini, D. (2022). Seismology on Mars: An analysis of direct, reflected, and converted seismic body waves with implications for interior structure. *Physics of the Earth and Planetary Interiors*, 325, 106851. https://doi.org/10.1016/j.pepi.2022.106851

BROOUET ET AL. 23 of 28

- Fa, W., & Wieczorek, M. A. (2012). Regolith thickness over the lunar nearside: Results from Earth-based 70-cm Arecibo radar observations. Icarus, 218(2), 771–787. https://doi.org/10.1016/j.icarus.2012.01.010
- Fassett, C., & Minton, D. (2013). Impact bombardment of the terrestrial planets and the early history of the Solar System. *Nature Geoscience*, 6(7), 520–524. https://doi.org/10.1038/ngeo1841
- Fleury, A., Plesa, A.-C., Tosi, N., Walterová, M., & Breuer, D. (2024). Variations of heat flux and elastic thickness of Mercury from 3-D thermal evolution modeling. *Geophysical Research Letters*, 51(21), e2024GL110622. https://doi.org/10.1029/2024GL110622
- Freed, A. M., Johnson, B. C., Blair, D. M., Melosh, H. J., Neumann, G. A., Phillips, R. J., et al. (2014). The formation of lunar mascon basins from impact to contemporary form. *Journal of Geophysical Research: Planets, 119*(11), 2378–2397. https://doi.org/10.1002/2014JE004657
- Ganesh, I., McGuire, L. A., & Carter, L. M. (2021). Modeling the dynamics of dense pyroclastic flows on Venus: Insights into pyroclastic eruptions. *Journal of Geophysical Research: Planets*, 126(9), e2021JE006943. https://doi.org/10.1029/2021JE006943
- Geng, M., Yang, Q., Kasmi, C., Welford, J. K., & Peace, A. L. (2024). Unveiling magmatic structures and connectivity beneath the lunar Oceanus Procellarum region from GRAIL gravity data. *Nature Communications*, 15(1), 10296. https://doi.org/10.1038/s41467-024-54692-2
- Genova, A. (2020). ORACLE: A mission concept to study Mars' climate, surface and interior. Acta Astronautica, 166, 317–329. https://doi.org/10.1016/j.actaastro.2019.10.006
- Genova, A., Goossens, S., Del Vecchio, E., Petricca, F., Beuthe, M., Wieczorek, M., et al. (2023). Regional variations of Mercury's crustal density and porosity from MESSENGER gravity data. *Icarus*, 391, 115332. https://doi.org/10.1016/j.icarus.2022.115332
- Genova, A., Goossens, S., Lemoine, F. G., Mazarico, E., Neumann, G. A., Smith, D. E., & Zuber, M. T. (2016). Seasonal and static gravity field of Mars from MGS, Mars Odyssey and MRO radio science. *Icarus*, 272, 228–245. https://doi.org/10.1016/j.icarus.2016.02.050
- Genova, A., Petricca, F., Andolfo, S., Gargiulo, A. M., Sulcanese, D., Mitri, G., & Chiarolanza, G. (2024). Water ice concentration and distribution in the Martian south polar layered deposits constrained by the lateral variations of their bulk density. *Icarus*, 414, 116025. https://doi.org/10.1016/j.jcarus.2024.116025
- Gilmore, M. S., Mueller, N., & Helbert, J. (2015). VIRTIS emissivity of Alpha Regio, Venus, with implications for Tessera composition. *Icarus*, 254, 350–361. https://doi.org/10.1016/j.icarus.2015.04.008
- Giuliani, F., Durante, D., Cascioli, G., De Marchi, F., Iess, L., Mazarico, E., & Smrekar, S. (2025). Mapping Venus's gravity field with the VERITAS mission. *Planetary Science Journal*, 6(1), 11. https://doi.org/10.3847/PSJ/ad991a
- Gong, S., Wieczorek, M. A., Nimmo, F., Kiefer, W. S., Head, J. W., Huang, C., et al. (2016). Thicknesses of mare basalts on the Moon from gravity and topography. *Journal of Geophysical Research: Planets*, 5, 854–870. https://doi.org/10.1002/2016je005008
- Goossens, S., Sabaka, T. J., Genova, A., Mazarico, E., Nicholas, J. B., & Neumann, G. A. (2017). Evidence for a low bulk crustal density for Mars from gravity and topography. *Geophysical Research Letters*, 44(15), 7686–7694. https://doi.org/10.1002/2017GL074172
- Goossens, S., Sabaka, T. J., Wieczorek, M. A., Neumann, G. A., Mazarico, E., Lemoine, F. G., et al. (2020). High-resolution gravity field models from GRAIL data and implications for models of the density structure of the Moon's crust. *Journal of Geophysical Research: Planets*, 125(2), e2019JE006086. https://doi.org/10.1029/2019JE006086
- Gülcher, A. J. P., Gerya, T., Montési, L. G. J., & Munch, J. (2020). Corona structures driven by plume–lithosphere interactions and evidence for ongoing plume activity on Venus. *Nature Geoscience*, 13(8), 547–554. https://doi.org/10.1038/s41561-020-0606-1
- Gyalay, S., Nimmo, F., Plesa, A.-C., & Wieczorek, M. (2020). Constraints on thermal history of Mars from depth of pore closure below InSight. Geophysical Research Letters, 47(16), e2020GL088653. https://doi.org/10.1029/2020GL088653
- Han, S.-C., Schmerr, N., Neumann, G., & Holmes, S. (2014). Global characteristics of porosity and density stratification within the lunar crust from GRAIL gravity and Lunar Orbiter Laser Altimeter topography data. Geophysical Research Letters, 41(6), 1882–1889. https://doi.org/10. 1002/2014GL059378
- Hauber, E., Brož, P., Jagert, F., Jodłowski, P., & Platz, T. (2011). Very recent and wide-spread basaltic volcanism on Mars. Geophysical Research Letters, 38(10), L10201. https://doi.org/10.1029/2011GL047310
- Head, J. W., Kreslavsky, M. A., & Pratt, S. (2002). Northern lowlands of Mars: Evidence for widespread volcanic flooding and tectonic deformation in the Hesperian Period. *Journal of Geophysical Research*, 107(E1), https://doi.org/10.1029/2000IE001445
- Hemingway, D. J., & Matsuyama, I. (2017). Isostatic equilibrium in spherical coordinates and implications for crustal thickness on the Moon, Mars, Enceladus, and elsewhere. Geophysical Research Letters, 44(15), 7695–7705. https://doi.org/10.1002/2017GL073334
- Herrick, R. R., & Phillips, R. J. (1992). Geological correlations with the interior density structure of Venus. *Journal of Geophysical Research*, 97(E10), 16017–16034. https://doi.org/10.1029/92JE01498
- Hess, P. C., & Head, J. W. (1990). Derivation of primary magmas and melting of crustal materials on Venus: Some preliminary petrogenetic considerations. *Earth, Moon, and Planets*, 50(1), 57–80. https://doi.org/10.1007/BF00142389
- Hikida, H., & Wieczorek, M. A. (2007). Crustal thickness of the Moon: New constraints from gravity inversions using polyhedral shape models. *Icarus*, 192(1), 150–166. https://doi.org/10.1016/j.icarus.2007.06.015
- Huang, Q., & Wieczorek, M. A. (2012). Density and porosity of the lunar crust from gravity and topography. *Journal of Geophysical Research*, 117(E5), E05003. https://doi.org/10.1029/2012JE004062
- Huang, Y. H., Soderblom, J. M., Minton, D. A., Hirabayashi, M., & Melosh, H. J. (2022). Bombardment history of the Moon constrained by crustal porosity. Nature Geoscience, 15(7), 531–535. https://doi.org/10.1038/s41561-022-00969-4
- Hynek, B. M., Beach, M., & Hoke, M. R. (2010). Updated global map of Martian valley networks and implications for climate and hydrologic processes. *Journal of Geophysical Research*, 115(E9). https://doi.org/10.1029/2009JE003548
- Iess, L., Asmar, S. W., Cappuccio, P., Cascioli, G., De Marchi, F., di Stefano, I., et al. (2021). Gravity, geodesy and fundamental physics with BepiColombo's MORE investigation. *Space Science Reviews*, 21(1), 21. https://doi.org/10.1007/s11214-021-00800-3
- Ito, K., & Kennedy, G. C. (1971). An experimental study of the basalt-garnet granulite-eclogite transition. In J. G. Heacock (Eds.), The structure and physical properties of the Earth's crust. https://doi.org/10.1029/GM014p0303
- James, P. B., Zuber, M. T., & Phillips, R. J. (2013). Crustal thickness and support of topography on Venus. *Journal of Geophysical Research: Planets*, 118(4), 859–875. https://doi.org/10.1029/2012JE004237
- James, P. B., Zuber, M. T., Phillips, R. J., & Solomon, S. C. (2015). Support of long-wavelength topography on Mercury inferred from MESSENGER measurements of gravity and topography. *Journal of Geophysical Research: Planets*, 120(2), 287–310. https://doi.org/10.1002/ 2014JE004713
- Jansen, J. C., Andrews-Hanna, J. C., Li, Y., Lucey, P., Taylor, G., Goossens, S., et al. (2017). Small-scale density variations in the lunar crust revealed by GRAIL. *Icarus*, 291, 107–123. https://doi.org/10.1016/j.icarus.2017.03.017
- Jozwiak, L. M., Head, J. W., Zuber, M. T., Smith, D. E., & Neumann, G. A. (2012). Lunar floor-fractured craters: Classification, distribution, origin and implications for magmatism and shallow crustal structure. *Journal of Geophysical Research*, 117(E11), E11005. https://doi.org/10.1029/20121F004134

BROOUET ET AL. 24 of 28

- Khan, A., & Mosegaard, K. (2002). An inquiry into the lunar interior: A nonlinear inversion of the Apollo lunar seismic data. *Journal of Geophysical Research*, 107(E6), 5036. https://doi.org/10.1029/2001JE001658
- Kiefer, W. S. (2013). Gravity constraints on the subsurface structure of the Marius Hills: The magmatic plumbing of the largest lunar volcanic dome complex. *Journal of Geophysical Research: Planets*, 118(4), 733–745. https://doi.org/10.1029/2012JE004111
- Kiefer, W. S., Macke, R. J., Britt, D. T., Irving, A. J., & Consolmagno, G. J. (2012). The density and porosity of lunar rocks. Geophysical Research Letters, 39(7), L07201. https://doi.org/10.1029/2012GL051319
- Kim, D., Duran, C., Giardini, D., Plesa, A.-C., Stähler, S. C., Boehm, C., et al. (2023). Global crustal thickness revealed by surface waves orbiting Mars. Geophysical Research Letters, 50(12), e2023GL103482. https://doi.org/10.1029/2023GL103482
- Kim, D., Lekić, V., Irving, J. C. E., Schmerr, N., Knapmeyer-Endrun, B., Joshi, R., et al. (2021). Improving constraints on planetary interiors with PPs receiver functions. *Journal of Geophysical Research: Planets*, 126(11), e2021F006983, https://doi.org/10.1029/2021F006983
- PPs receiver functions. Journal of Geophysical Research: Planets, 126(11), e2021JE006983. https://doi.org/10.1029/2021JE006983
 Knapmeyer-Endrun, B., Adam, L., Carrasco, S., Golombek, M. P., Kim, D., Knapmeyer, M., et al. (2025). Porosity and hydrous alteration of the
- Martian crust from InSight seismic data. *Physics of the Earth and Planetary Interiors*, 366, 107383. https://doi.org/10.1016/j.pepi.2025.107383 Knapmeyer-Endrun, B., Panning, M. P., Bissig, F., Joshi, R., Khan, A., Kim, D., et al. (2021). Thickness and structure of the Martian crust from InSight seismic data. *Science*, 373(6553), 438–443. https://doi.org/10.1126/science.abf8966
- Konopliv, A. S., Banerdt, W. B., & Sjogren, W. L. (1999). Venus gravity: 180th degree and order model. Icarus, 139(1), 3–18. https://doi.org/10.1006/icar.1999.6086
- Konopliv, A. S., Park, R. S., & Ermakov, A. I. (2020). The Mercury gravity field, orientation, love number, and ephemeris from the MESSENGER radiometric tracking data. *Icarus*, 335, 113386. https://doi.org/10.1016/j.icarus.2019.07.020
- Kucinskas, A. B., & Turcotte, D. L. (1994). Isostatic compensation of equatorial highlands on Venus. *Icarus*, 1, 104–116. https://doi.org/10.1006/jcar.1994.1172
- Laneuville, M., Taylor, J., & Wieczorek, M. A. (2018). Distribution of radioactive heat sources and thermal history of the Moon. *Journal of Geophysical Research: Planets*, 123(12), 3144–3166. https://doi.org/10.1029/2018JE005742
- Laneuville, M., Wieczorek, M. A., Breuer, D., & Tosi, N. (2013). Asymmetric thermal evolution of the Moon. *Journal of Geophysical Research:* Planets, 118(7), 1435–1452. https://doi.org/10.1002/jgre.20103
- Langlais, B., Lesur, V., Purucker, M., Connerney, J. E. P., & Mandea, M. (2010). Crustal magnetic fields of terrestrial planets. Space Science Reviews. 152(1–4), 223–249. https://doi.org/10.1007/s11214-009-9557-v
- Lewis, K. W., Peters, S., Gonter, K., Morrison, S., Schmerr, N., Vasavada, A. R., & Gabriel, T. (2019). A surface gravity traverse on Mars indicates low bedrock density at Gale crater. Science, 363(6426), 535–537. https://doi.org/10.1126/science.aat0738
- Li, J., Beghein, C., McLennan, S. M., Horleston, A. C., Charalambous, C., Huang, Q., et al. (2022). Constraints on the Martian crust away from the InSight landing site. *Nature Communications*, 13(1), 7950. https://doi.org/10.1038/s41467-022-35662-y
- Li, Y., & Oldenburg, D. W. (1998). 3-D inversion of gravity data. Geophysics, 63(1), 109-119. https://doi.org/10.1190/1.1444302
- Liang, Q., Chen, C., & Li, Y. (2014). 3-D inversion of gravity data in spherical coordinates with application to the GRAIL data. *Journal of Geophysical Research: Planets*, 119(6), 1359–1373. https://doi.org/10.1002/2014JE004626
- Lognonné, P., Gagnepain-Beyneix, J., & Chenet, H. (2003). A new seismic model of the Moon: Implications for structure, thermal evolution and formation of the Moon. *Earth and Planetary Science Letters*, 211(1–2), 27–44. https://doi.org/10.1016/S0012-821X(03)00172-9
- Lognonné, P., & Johnson, C. (2015). Planetary seismology. In *Treatise on geophysics* (2nd ed., Vol. 10, pp. 65–120). https://doi.org/10.1016/B978-0-444-53802-4.00167-6
- Lourenço, D. J., Rozel, A. B., Ballmer, M. D., & Tackley, P. J. (2020). Plutonic-squishy lid: A new global tectonic regime generated by intrusive magmatism on Earth-like planets. Geochemistry, Geophysics, Geosystems, 21(4), e2019GC008756. https://doi.org/10.1029/2019GC008756
- Maia, J. S., & Wieczorek, M. A. (2022). Lithospheric structure of Venusian crustal plateaus. *Journal of Geophysical Research: Planets*, 127(2), e2021JE007004. https://doi.org/10.1029/2021JE007004
- Maia, J. S., Wieczorek, M. A., & Plesa, A.-C. (2023). The mantle viscosity structure of Venus. Geophysical Research Letters, 50(15), e2023GL103847. https://doi.org/10.1029/2023GL103847
- Marchi, S., Chapman, C. R., Fassett, C. I., Head, J. W., Bottke, W. F., & Strom, R. G. (2013). Global resurfacing of Mercury 4.0-4.1 billion years ago by heavy bombardment and volcanism. *Nature*, 499(7456), 59–61. https://doi.org/10.1038/nature12280
- Mazarico, E., Genova, A., Goossens, S., Lemoine, F. G., Neumann, G. A., Zuber, M. T., et al. (2014). The gravity field, orientation, and ephemeris of Mercury from MESSENGER observations after three years in orbit. *Journal of Geophysical Research: Planets*, 119(12), 2417–2436. https://doi.org/10.1002/2014JE004675
- McGovern, P. J., Solomon, S. C., Smith, D. E., Zuber, M. T., Simons, M., Wieczorek, M. A., et al. (2002). Localized gravity/topography admittance and correlation spectra on Mars: Implications for regional and global evolution. *Journal of Geophysical Research*, 107(E12). https://doi.org/10.1029/2002JE001854
- McKay, D. S., Heiken, G., Basu, A., Blanford, G., Simons, S., Reedy, R., et al. (1991). The lunar regolith. In *Lunar sourcebook* (Vol. 567, pp. 285–356)
- McLennan, S. M. (2022). Composition of planetary crusts and planetary differentiation. In *Planetary Volcanism across the solar system* (Vol. 1, pp. 287–331). https://doi.org/10.1016/B978-0-12-813987-5.00008-0
- Melosh, H. J., Freed, A. M., Johnson, B. C., Blair, D. M., Andrews-Hanna, J. C., Neumann, G. A., et al. (2013). The origin of lunar mascon basins. Science, 340(6140), 1552–1555. https://doi.org/10.1126/science.1235768
- Metzger, P. T., Grundy, W. M., Sykes, M. V., Stern, A., Bell, J. F., III., Detelich, C. E., et al. (2022). Moons are planets: Scientific usefulness versus cultural teleology in the taxonomy of planetary science. *Icarus*, 374, 114768. https://doi.org/10.1016/j.icarus.2021.114768
- Michalski, J. R., Rogers, D. A., Edwards, C. S., Cowart, A., & Xiao, L. (2024). Diverse volcanism and crustal recycling on early Mars. Nature Astronomy, 8(4), 456–462. https://doi.org/10.1038/s41550-023-02191-7
- Michaut, C., & Neufeld, J. A. (2022). Formation of the lunar primary crust from a long-lived slushy magma ocean. *Geophysical Research Letters*, 49(2), e2021GL095408. https://doi.org/10.1029/2021GL095408
- Miljković, K., Wieczorek, M. A., Collins, G. S., Laneuville, M., Neumann, G. A., Melosh, H. J., et al. (2013). Asymmetric distribution of lunar impact basins caused by variations in target properties. *Science*, 342(6159), 724–726. https://doi.org/10.1126/science.1243224
- Mittelholz, A., Moorkamp, M., Broquet, A., & Ojha, L. (2025). Gravity and magnetic field signatures in hydrothermally affected regions on Mars. Journal of Geophysical Research: Planets, 130(4), e2024JE008832. https://doi.org/10.1029/2024JE008832
- Mohit, P. S., & Phillips, R. J. (2006). Viscoelastic evolution of lunar multiring basins. *Journal of Geophysical Research*, 111(E12), E12001. https://doi.org/10.1029/2005JE002654
- Mohit, P. S., & Phillips, R. J. (2007). Viscous relaxation on early Mars: A study of ancient impact basins. *Geophysical Research Letters*, 34(21), L21204. https://doi.org/10.1029/2007GL031252
- Mohorovičić, A. (1992). Earthquake of 8 October 1909 (translation in English). Geofizika, 9, 3–55.

BROOUET ET AL. 25 of 28

- Mooney, W. D., Barrera-Lopez, C., Suárez, M. G., & Castelblanco, M. A. (2023). Earth crustal model 1 (ECM1): A 1° × 1° global seismic and density model. *Earth-Science Reviews*, 243, 104493. https://doi.org/10.1016/j.earscirev.2023.104493
- Namiki, N., Iwata, T., Matsumoto, K., Hanada, H., Noda, H., Goossens, S., et al. (2009). Farside gravity field of the Moon from four-way Doppler measurements of SELENE (Kaguya). Science, 323(5916), 900–905. https://doi.org/10.1126/science.1168029
- Neumann, G. A., Zuber, M. T., Smith, D. E., & Lemoine, F. G. (1996). The lunar crust: Global structure and signature of major basins. *Journal of Geophysical Research*, 101(E7), 16841–16843. https://doi.org/10.1029/96JE01246
- Neumann, G. A., Zuber, M. T., Wieczorek, M. A., McGovern, P. J., Lemoine, F. G., & Smith, D. E. (2004). Crustal structure of Mars from gravity and topography. *Journal of Geophysical Research*, 109(E8), E08002. https://doi.org/10.1029/2004JE002262
- Nimmo, F., & Mackwell, S. (2023). Viscous relaxation as a probe of heat flux and crustal plateau composition on Venus. *Proceedings of the National Academy of Sciences of the United States of America*, 120(3), e2216311120. https://doi.org/10.1073/pnas.2216311120
- Nimmo, F., & Pappalardo, R. T. (2016). Ocean worlds in the outer solar system. *Journal of Geophysical Research: Planets*, 121(8), 1378–1399. https://doi.org/10.1002/2016JE005081
- Nimmo, F., & Stevenson, D. J. (2001). Estimates of Martian crustal thickness from viscous relaxation of topography. *Journal of Geophysical Research*, 106(E3), 5085–5098. https://doi.org/10.1029/2000JE001331
- Ojha, L., & Lewis, K. (2018). The density of the Medusae Fossae Formation: Implications for its composition, origin, and importance in Martian history. *Journal of Geophysical Research: Planets*, 123(6), 1368–1379. https://doi.org/10.1029/2018JE005565
- Padovan, S., Wieczorek, M. A., Margot, J., Tosi, N., & Solomon, S. C. (2015). Thickness of the crust of Mercury from geoid-to-topography ratios. Geophysical Research Letters, 42(4), 1029–1038. https://doi.org/10.1002/2014GL062487
- Panning, M. P., Kedar, S., Aboobaker, A., Aveni, G., Biernacki, K., Bowles, N., et al. (2024). Farside seismic suite: InSight's Sequel on the Moon. In 55th Lunar & Planetary Science Conference (Vol. 6050).
- Park, R. S., Berne, A., Konopliv, A. S., Keane, J. T., Matsuyama, I., Nimmo, F., et al. (2025). Thermal asymmetry in the Moon's mantle inferred
- from monthly tidal response. Nature, 641(8065), 1188–1192. https://doi.org/10.1038/s41586-025-08949-5
 Parker, R. L. (1973). The rapid calculation of potential anomalies. Geophysical Journal of the Royal Astronomical Society, 31(4), 447–455. https://
- doi.org/10.1111/j.1365-246X.1973.tb06513.x
 Pauer, M., Fleming, K., & Čadek, O. (2006). Modeling the dynamic component of the geoid and topography of Venus. *Journal of Geophysical*
- Research, 111(E11), E11012. https://doi.org/10.1029/2005JE002511
 Phillips, R. J., & Lambeck, K. (1980). Gravity fields of the terrestrial planets: Long-wavelength anomalies and tectonics. Reviews of Geophysics,
- 18(1), 27–76. https://doi.org/10.1029/rg018i001p00027
 Phillips, R. J., Zuber, M. T., Solomon, S. C., Golombek, M. P., Jakosky, B. M., Banerdt, W. B., et al. (2001). Ancient geodynamics and global-
- scale hydrology on Mars. Science, 291(5513), 2587–2591. https://doi.org/10.1126/science.1058701
- Phipps Morgan, J., & Blackman, D. K. (1993). Inversion of combined gravity and bathymetry data for crustal structure: A prescription for downward continuation. Earth and Planetary Science Letters, 119(1–2), 167–179. https://doi.org/10.1016/0012-821X(93)90014-Z
- Plesa, A.-C., Padovan, S., Tosi, N., Breuer, D., Grott, M., Wieczorek, M. A., et al. (2018). The thermal state and interior structure of Mars. Geophysical Research Letters, 45(22), 12198–12209. https://doi.org/10.1029/2018GL080728
- Plesa, A.-C., Wieczorek, M. A., Knapmeyer, M., Rivoldini, A., Walterová, M., & Breuer, D. (2022). Chapter Four—Interior dynamics and thermal evolution of Mars—A geodynamic perspective. *Advances in Geophysics*, 63. https://doi.org/10.1016/bs.agph.2022.07.005
- Qian, Y., Xiao, L., Head, J. W., van der Bogert, C. H., Hiesinger, H., & Wilson, L. (2021). Young lunar mare basalts in the Chang'E-5 sample return region, northern Oceanus Procellarum. Earth and Planetary Science Letters, 555, 116702. https://doi.org/10.1016/j.epsl.2020.116702
- Richards, M. A., & Hager, B. H. (1984). Geoid anomalies in a dynamic Earth. *Journal of Geophysical Research*, 89(B7), 5987–6002. https://doi.org/10.1029/JB089iB07p05987
- Ritzer, J. A., & Hauck, S. A. (2009). Lithospheric structure and tectonics at Isidis Planitia, Mars. *Icarus*, 201(2), 528–539. https://doi.org/10.1016/j.icarus.2009.01.025
- Roberts, J. H., McKinnon, W. B., Elder, C. M., Tobie, G., Biersteker, J. B., Young, D., et al. (2023). Exploring the interior of Europa with the Europa Clipper. Space Science Reviews, 219(6), 46. https://doi.org/10.1007/s11214-023-00990-y
- Rodriguez, J. A. P., Dobrea, E. N., Kargel, J. S., Baker, V. R., Crown, D. A., Webster, K. D., et al. (2020). The oldest highlands of Mars may be massive dust fallout deposits. *Scientific Reports*, 10(1), 10347. https://doi.org/10.1038/s41598-020-64676-z
- Rosenblatt, P., Dumoulin, C., Marthy, J. C., & Genova, A. (2021). Determination of Venus' interior structure with EnVision. *Remote Sensing*, 13(9), 1624. https://doi.org/10.3390/rs13091624
- Sautter, V., Toplis, M., Wiens, R., Cousin, A., Fabre, C., Gasnault, O., et al. (2015). In situ evidence for continental crust on early Mars. *Nature Geoscience*, 8, 605–609. https://doi.org/10.1038/ngeo2474
- Smith, D. E., Zuber, M. T., Frey, H. V., Garvin, J. B., Head, J. W., Muhleman, D. O., et al. (2001). Mars orbiter laser altimeter: Experiment summary after the first year of global mapping of Mars. *Journal of Geophysical Research*, 106(E10), 23689–23722. https://doi.org/10.1029/2000JE001364
- Smith, D. E., Zuber, M. T., Neumann, G. A., Lemoine, F. G., Mazarico, E., Torrence, M. H., et al. (2010). Initial observations from the lunar orbiter laser altimeter (LOLA). *Geophysical Research Letters*, 37(18), L18204. https://doi.org/10.1029/2010GL043751
- Smith, M., Craig, D., Herrmann, N., Mahoney, E., Krezel, J., McIntyre, N., & Goodliff, K. (2020). The Artemis program: An overview of NASA's activities to return humans to the Moon. In 2020 IEEE Aerospace Conference. https://doi.org/10.1109/AERO47225.2020.9172323
- Smrekar, S., Hensley, S., Nybakken, R., Wallace, M. S., Perkovic-Martin, D., You, T.-H., et al. (2022). VERITAS (Venus emissivity, radio science, InSAR, topography, and spectroscopy): A Discovery mission. In 2022 IEEE Aerospace Conference. https://doi.org/10.1109/AERO53065.2022.9843269
- Smrekar, S. E., Ostberg, C., & O'Rourke, J. G. (2023). Earth-like lithospheric thickness and heat flow on Venus consistent with active rifting. Nature Geoscience, 16(1), 13–18. https://doi.org/10.1038/s41561-022-01068-0
- Smrekar, S. E., & Phillips, R. J. (1991). Venusian highlands: Geoid to topography ratios and their implications. *Earth and Planetary Science Letters*, 107(3–4), 582–597. https://doi.org/10.1016/0012-821X(91)90103-O
- Solomon, S. C., & Head, J. W. (1980). Lunar mascon basins: Lava filling, tectonics, and evolution of the lithosphere. *Reviews of Geophysics*, 18(1), 107–141. https://doi.org/10.1029/RG018i001p00107
- Sori, M. M. (2018). A thin, dense crust for Mercury. Earth and Planetary Science Letters, 489, 92–99. https://doi.org/10.1016/j.epsl.2018.02.033 Spencer, C. J., Roberts, N. M. W., & Santosh, M. (2017). Growth, destruction, and preservation of Earth's continental crust. Earth-Science Reviews, 172, 87–106. https://doi.org/10.1016/j.earscirev.2017.07.013
- Šprlák, M., Han, S.-C., & Featherstone, W. E. (2020). Crustal density and global gravitational field estimation of the Moon from GRAIL and LOLA satellite data. *Planetary and Space Science*, 192, 105032. https://doi.org/10.1016/j.pss.2020.105032

BROOUET ET AL. 26 of 28

- Stolper, E., & Walker, D. (1980). Melt density and the average composition of basalt. Contributions to Mineralogy and Petrology, 1, 7–12. https://doi.org/10.1007/bf00375484
- Surkov, Y. A., Barsukov, V. L., Moskalyeva, L. P., Kharyukova, V. P., & Kemurdzhian, A. L. (1984). New data on the composition, structure, and properties of Venus rock obtained by Venera 13 and Venera 14. *Journal of Geophysical Research*, 89(S02), B393–B402. https://doi.org/10.1029/JB089iS02p0B393
- Surkov, Y. A., Moskalyova, L. P., Kharyukova, V. P., Dudin, A. D., Smirnov, G. G., & Zaitseva, S. Y. (1986). Venus rock composition at the Vega 2 landing site. *Journal of Geophysical Research*, 91(B13), E215–E218. https://doi.org/10.1029/JB091iB13p0E215
- Tanaka, K. L., Skinner, J. A., Dohm, J. M., Irwin, R. P., Kolb, E. J., Fortezzo, C. M., et al. (2014). Geologic map of Mars: U.S. geological survey scientific investigations map 3292, scale 1:20,000,000. US Geol. Surv. Geol. Investig. https://doi.org/10.3133/sim3292
- Taylor, G. J., Boynton, W., Brückner, J., Wänke, H., Dreibus, G., Kerry, K., et al. (2006). Bulk composition and early differentiation of Mars. *Journal of Geophysical Research*, 111(E3). https://doi.org/10.1029/2005JE002645
- Taylor, G. J., & Wieczorek, M. A. (2014). Lunar bulk chemical composition: A post-gravity recovery and interior laboratory reassessment. Philosophical Transactions of the Royal Society A, 372(2024), 20130242. https://doi.org/10.1098/rsta.2013.0242
- Taylor, S. R., & McLennan, S. M. (2009). Planetary crusts: Their composition, origin and evolution. Cambridge University Press.
- Thomas, N., Hussmann, H., Spohn, T., Lara, L. M., Christensen, U., Affolter, M., et al. (2021). The BepiColombo laser altimeter. *Space Science Reviews*, 217(1), 25. https://doi.org/10.1007/s11214-021-00794-y
- Thorey, C., Michaut, C., & Wieczorek, M. A. (2015). Gravitational signatures of lunar floor-fractured craters. Earth and Planetary Science Letters, 424, 269–279. https://doi.org/10.1016/j.epsl.2015.04.021
- Tosi, N., Čadek, O., Běhounková, M., Kanova, M., Plesa, A.-C., Grott, M., et al. (2015). Mercury's low-degree geoid and topography controlled by insolation-driven elastic deformation. *Geophysical Research Letters*, 42, 7327–7335. https://doi.org/10.1002/2015GL065314
- Turcotte, D. L., Shcherbakov, R., Malamud, B. D., & Kucinskas, A. B. (2002). Is the Martian crust also the Martian elastic lithosphere? *Journal of Geophysical Research*, 107(E11), 5091. https://doi.org/10.1029/2001JE001594
- Turcotte, D. L., Willemann, R. J., Haxby, W. F., & Norberry, J. (1981). Role of membrane stresses in the support of planetary topography. *Journal of Geophysical Research*, 86(B5), 3951–3959. https://doi.org/10.1029/JB086iB05p03951
- Uieda, L., Barbosa, V. C. F., & Braitenberg, C. (2016). Tesseroids: Forward-modeling gravitational fields in spherical coordinates. *Geophysics*, 81(5), F41–F48. https://doi.org/10.1190/geo2015-0204.1
- Van Hoolst, T., Tobie, G., Vallat, C., Altobelli, N., Bruzzone, L., Cao, H., et al. (2024). Geophysical characterization of the interiors of Ganymede, Callisto and Europa by ESA's JUpiter ICy moons explorer. Space Science Reviews, 220(5), 54. https://doi.org/10.1007/s11214-024-01085-y Venkatadri, T., & James, P. (2020). Variations of porosity in intermediate-sized lunar impact basins. Icarus, 352, 113953. https://doi.org/10.1016/
- Voigt, J. R. C., Hamilton, C. W., Steinbrügge, G., Christoffersen, M. S., Nerozzi, S., Kerber, L., et al. (2023). Revealing Elysium Planitia's young geologic history: Constraints on lava emplacement, areas, and volumes. *Journal of Geophysical Research: Planets*, 128(12), e2023JE007947.
- https://doi.org/10.1029/2023JE007947
 Wahl, D., Wieczorek, M. A., Wünnemann, K., & Oberst, J. (2020). Crustal porosity of lunar impact basins. *Journal of Geophysical Research:*
- Planets, 125(4), e2019JE006335. https://doi.org/10.1029/2019JE006335
 Warren, P. H., & Rasmussen, K. L. (1987). Megaregolith insulation, internal temperatures, and bulk uranium content of the Moon. Journal of Geophysical Research, B5, 3453–3465. https://doi.org/10.1029/jb092ib05p03453
- Watters, T. R., James, P. B., & Selvans, M. M. (2021). Mercury's crustal thickness and contractional strain. *Geophysical Research Letters*, 48(17), e2021GL093528. https://doi.org/10.1029/2021GL093528
- Watts, A. B. (2015). Crustal and lithosphere dynamics: An introduction and overview. In *Treatise on geophysics* (2nd ed., Vol. 6, pp. 1–44). https://doi.org/10.1016/B978-0-444-53802-4.00110-X
- White, S. M., Crisp, J. A., & Spera, F. J. (2006). Long-term volumetric eruption rates and magma budgets. *Geochemistry, Geophysics, Geosystems*, 7(3), O03010. https://doi.org/10.1029/2005GC001002
- Widemann, T., Smrekar, S. E., Garvin, J. B., Straume-Lindner, A. G., Ocampo, A. C., Schulte, M. D., et al. (2023). Venus evolution through time: Key science questions, selected mission concepts and future investigations. *Space Science Reviews*, 219(7), 56. https://doi.org/10.1007/s11214-023-02002-w
- Wieczorek, M. A. (2008). Constraints on the composition of the Martian south polar cap from gravity and topography. *Icarus*, 196(2), 506–517. https://doi.org/10.1016/i.Icarus.2007.10.026
- Wieczorek, M. A. (2015). Gravity and topography of the terrestrial planets. Treatise on Geophysics, 153–193. https://doi.org/10.1016/b978-0-444-53802-4.00169-x
- Wieczorek, M. A. (2024). MarkWieczorek/ctplanet: Version 0.2.14. Zenodo. https://doi.org/10.5281/zenodo.14582868
- Wieczorek, M. A., Beuthe, M., Rivoldini, A., & Van Hoolst, T. (2019). Hydrostatic interfaces in bodies with nonhydrostatic lithospheres. *Journal of Geophysical Research: Planets*, 124(5), 1410–1432. https://doi.org/10.1029/2018JE005909
- Wieczorek, M. A., Broquet, A., McLennan, S. M., Rivoldini, A., Golombek, M., Antonangeli, D., et al. (2022). InSight constraints on the global character of the Martian crust. *Journal of Geophysical Research: Planets*. 127(5), e2022JE007298. https://doi.org/10.1029/2022JE007298
- Wieczorek, M. A., Meschede, M., Broquet, A., Brugere, T., Corbin, A., EricAtORS, et al. (2024). SHTOOLS: Version 4.13. Zenodo. https://doi.org/10.5281/zenodo.592762
- Wieczorek, M. A., Neumann, G. A., Nimmo, F., Kiefer, W. S., Taylor, G. J., Melosh, H. J., et al. (2013). The crust of the Moon as seen by GRAIL. Science, 339(6120), 671–675. https://doi.org/10.1126/science.1231530
- Wieczorek, M. A., & Phillips, R. J. (1998). Potential anomalies on a sphere: Applications to the thickness of the lunar crust. *Journal of Geophysical Research*, 103(E1), 1715–1724. https://doi.org/10.1029/97JE03136
- Wieczorek, M. A., & Phillips, R. J. (1999). Lunar multiring basins and the cratering process. *Icarus*, 139(2), 246–259. https://doi.org/10.1006/icar.
- Wieczorek, M. A., & Phillips, R. J. (2000). The "Procellarum KREEP Terrane": Implications for mare volcanism and lunar evolution. *Journal of Geophysical Research*, 105(E8), 20417–20430. https://doi.org/10.1029/1999JE001092
- Wieczorek, M. A., & Simons, F. J. (2005). Localized spectral analysis on the sphere. Geophysical Journal International, 162(3), 655–675. https://doi.org/10.1111/j.1365-246X.2005.02687.x
- Wieczorek, M. A., & Zuber, M. T. (2004). Thickness of the Martian crust: Improved constraints from geoid-to-topography ratios. *Journal of Geophysical Research*, 109(E1), E01009. https://doi.org/10.1029/2003JE002153
- Wiggins, S. E., Johnson, B. C., Collins, G. S., Jay Melosh, H., & Marchi, S. (2022). Widespread impact-generated porosity in early planetary crusts. *Nature Communications*, 13(1), 4817. https://doi.org/10.1038/s41467-022-32445-3

BROOUET ET AL. 27 of 28

- Wood, J. A., Dickey, J. S., Marvin, U. B., & Powell, B. N. (1970). Lunar anorthosites. Science, 167(3918), 602–604. https://doi.org/10.1126/science.167.3918.602
- Wörner, L., Root, B., Bouyer, P., Braxmaier, C., Dirkx, D., Encarnação, J., et al. (2023). MaQuIs—Concept for a Mars quantum gravity mission. Planetary and Space Science, 239, 105800. https://doi.org/10.1016/j.pss.2023.105800
- Yamamoto, S., Nakamura, R., Matsunaga, T., Ogawa, Y., Ishihara, Y., Morota, T., et al. (2010). Possible mantle origin of olivine around lunar impact basins detected by SELENE. *Nature Geoscience*, 3(8), 533–536. https://doi.org/10.1038/ngeo897
- Zhao, G., Chen, B., Uieda, L., Liu, J., Kaban, M. K., Chen, L., & Guo, R. (2019). Efficient 3-D large-scale forward modeling and inversion of gravitational fields in spherical coordinates with application to lunar mascons. *Journal of Geophysical Research: Solid Earth*, 124(4), 4157–4173. https://doi.org/10.1029/2019JB017691
- Zhou, W.-Y., Olson, P. L., Shearer, C. K., Agee, C. B., Townsend, J. P., Hao, M., et al. (2022). High pressure-temperature phase equilibrium studies on Martian basalts: Implications for the failure of plate tectonics on Mars. *Earth and Planetary Science Letters*, 594, 117751. https://doi.org/10.1016/j.epsl.2022.117751
- Zhu, M. H., Ding, M., Wieczorek, M., Morbidelli, A., Xu, L., & Yin, Q. Z. (2025). Obliteration of ancient impact basins on the Moon by viscous relaxation. *Nature Astronomy*, 9(3), 333–346. https://doi.org/10.1038/s41550-024-02444-z
- Zuber, M. T., Phillips, R. J., Andrews-Hanna, J. C., Asmar, S. W., Konopliv, A. S., Lemoine, F. G., et al. (2007). Density of Mars' south polar layered deposits. Science, 317(5845), 1718–1719. https://doi.org/10.1126/science.1146995
- Zuber, M. T., Smith, D. E., Watkins, M. M., Asmar, S. W., Konopliv, A. S., Lemoine, F. G., et al. (2013). Gravity field of the Moon from the gravity recovery and interior laboratory (GRAIL) mission. *Science*, 339(6120), 668–671. https://doi.org/10.1126/science.1231507

Erratum

The originally published version of this article omitted the following from the end of the Acknowledgments: "The authors thank Associate Editor Mike Sori, Reviewer Peter James, and an anonymous reviewer for their detailed comments, which helped improve the manuscript." The error has been corrected, and this may be considered the authoritative version of record.

BROQUET ET AL. 28 of 28